
Interpretable Neural ODEs for Gene Regulatory Network Discovery under Perturbations

Zaikang Lin *

New York Genome Center
Helmholtz Munich
z13135@columbia.edu

Sei Chang *

New York Genome Center
Columbia University
shc2170@columbia.edu

Aaron Zweig

New York Genome Center
Columbia University
az2888@columbia.edu

Minseo Kang

New York Genome Center
Columbia University
mk4554@columbia.edu

Elham Azizi

Irving Institute for Cancer Dynamics
Columbia University
ea2690@columbia.edu

David A. Knowles

New York Genome Center
Columbia University
dak2173@columbia.edu

Abstract

Modern high-throughput biological datasets with thousands of perturbations provide the opportunity for large-scale discovery of causal graphs that represent regulatory interactions between genes. Differentiable causal graphical models have been proposed to infer a gene regulatory network (GRN) from large-scale interventional datasets, capturing causal gene regulatory relationships from genetic perturbations. However, existing models are limited in scalability and fail to address the dynamic nature of biological processes such as cellular differentiation. We propose *PerturbODE*, a novel framework that incorporates interpretable neural ordinary differential equations (neural ODEs) to model cell state trajectories under perturbations and derive the causal GRN from the neural ODE’s parameters, enabling downstream simulation of unseen genetic interventions. We demonstrate *PerturbODE*’s efficacy in trajectory prediction and GRN inference across simulated and real overexpression datasets.

1 Introduction

GRNs capture the complex regulatory interactions between genes that dictate cell function, development, and responses to environmental changes. High-throughput perturbation assays with single-cell RNA sequencing (scRNA-seq) readouts, such as Perturb-seq [Dixit et al., 2016] or open reading frame (ORF) overexpression [Joung et al., 2023], enable precise measurement of gene expression changes across cell types resulting from genetic perturbations. However, inferring GRNs from scRNA-seq experiments remains challenging due to the problem’s exponential search space.

Regression-based approaches train a separate regression for each gene from all other genes, with random forests showing particular promise (e.g., GENIE3). While these simple approaches have performed well on some GRN recovery benchmarks [Pratapa et al., 2020, Huynh-Thu et al., 2010],

* Equal Contribution

they cannot distinguish between direct and mediated causal effects, account for latent confounding, or generalize to unseen interventions.

In contrast, recent causal graphical models have been developed to leverage the increasing availability of perturbational datasets in single-cell genomics. Their explicit encoding of the relationships between causal variables (genes) enables them to generate samples from learned interventional distributions [Tejada-Lapuerta et al., 2023]. Causal models enable tractable network inference through a continuous, albeit non-convex, optimization program that learns a directed acyclic graph (DAG) corresponding to the underlying GRN [Zheng et al., 2018, Fang et al., 2023, Brouillard et al., 2020, Lopez et al., 2022].

Causal graphical models have focused on learning structure from CRISPR-based gene knockdown or overexpression-based Perturb-seq. These perturbations are modest, slightly shifting cell state but not pushing cells into distinct cell types. However, new ORF overexpression single-cell experiments provide large perturbations, providing insights into previously unexplored aspects of dynamic gene regulation during differentiation. In particular, the Transcription Factor (TF) Atlas applied single-cell resolution assays to systematically study the effects of overexpression of 1,836 TFs in embryonic stem cells, generating more than 1.1 million cell profiles measured 7 days after TF perturbation [Joung et al., 2023]. TFs, proteins that bind to the genome to regulate gene expression, play a crucial role in defining cell states. TF overexpression can induce significant changes in cell fate that mimick those of natural development, allowing us to model how TFs direct stem cells along trajectories into diverse differentiated cell types such as myocytes and neurons. Since gene regulation during differentiation is inherently dynamic, accurately capturing these dynamics is essential to effectively modeling interventional distributions under TF overexpression. Extensive fluorescent experiments in yeast and *E. coli* have demonstrated that gene regulatory dynamics can be effectively modeled by nonlinear dynamical systems [Alon, 2006, Setty et al., 2003, Kalir and Alon, 2004].

Causal graphical models are limited in their ability to model the full complexity of high-dimensional interventional data that capture dynamic biological processes. To address these limitations, we propose *PerturbODE*, a novel neural ODE-based framework that 1) explicitly encodes the GRN in its parameters, enabling simultaneous trajectory inference and GRN discovery, 2) maps cell states into a lower dimensional “gene module” space analogously to causal representation learning (CRL) in Schölkopf et al. [2021], 3) allows explicit input of which gene(s) were perturbed, a feature uncommon in CRL approaches, 4) can model cycles and non-linear gene interactions, and 5) leverage causal relationships to predict the effects of unseen perturbations. Trained on the TF Atlas scRNA-seq data that capture the differentiation pathways of cells perturbed by overexpression of over a thousand TFs, *PerturbODE* enables scalable and interpretable discovery of the gene dependencies that drive cellular differentiation.

2 Related Work

Causal graph discovery from genetic perturbations. Structure learning of causal graphs has recently been applied to Perturb-seq interventional experiments to infer an underlying GRN. The nodes in the encoded causal graph correspond to genes, and the directed edges ideally correspond to direct causal regulatory relationships between genes. Since the number of possible DAGs grows exponentially with the number of nodes, classical causal graph discovery approaches cannot scale beyond a modest number of genes (typically 50-200). NO-TEARS [Zheng et al., 2018] introduced a continuous optimization objective via the trace exponential acyclicity constraint, significantly simplifying the problem complexity and enabling gradient descent-based structure learning. Extensions have further improved scalability. NO-TEARS-LR [Fang et al., 2024] adds a low-rank assumption to NO-TEARS to efficiently infer large and dense DAGs. DCDI [Brouillard et al., 2020] extends the continuous optimization formulation to interventional data but can only scale up to 50 dimensions in their original implementation with the trace exponential acyclicity constraint. DCDFG [Lopez et al., 2022] addresses DCDI’s limited scalability by employing a low-rank factor graph structure and spectral radius acyclicity constraint.

Neural ODEs for cell trajectory inference and modeling gene regulation. Differential equation-based models have long been considered the gold standard for modeling gene regulation due to their fidelity to our understanding of true biophysical mechanisms. Neural ODEs allow flexible parameterization and efficient training with differentiable ODE integration-solvers (e.g., via the

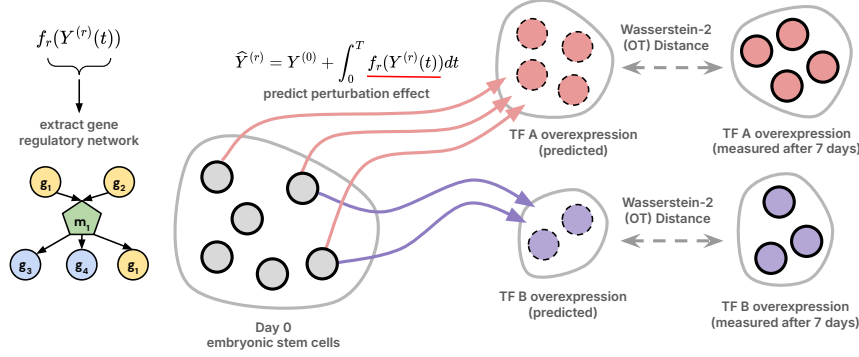


Figure 1: PerturbODE models the effect of a TF perturbation on stem cell differentiation by integrating the learned neural ODE function f from the initial cell states $Y^{(0)}$ under intervention I_r . The predicted final cell states $\hat{Y}^{(r)}$ are then compared to the observed differentiated gene expression values using the Wasserstein distance. From the parameters of f , we extract an underlying GRN.

adjoint method), allowing tractable mechanistic modeling of dynamics given data [Chen et al., 2018]. Neural ODEs and their stochastic variants have been applied to trajectory inference, where the continuous development of cellular states is mapped over time. Jackson et al. [2023] parameterizes ODEs with recurrent neural networks (RNNs) to model dynamics before obtaining the coefficient of partial determination to represent the contribution of each TF. Hossain et al. [2024] incorporates kinetics using biological priors (e.g., using the Hill function) and explicitly encodes the GRN as model parameters, but requires densely sampled data points along a pseudotime trajectory. However, both methods are designed to learn from a single experimental environment and cannot leverage information from multiple interventions.

Causal graph learning through stationary diffusion. The recently proposed method Bicycle Rohbeck et al. [2024] considers the GRN as the linear drift of a stable Ornstein-Uhlenbeck (OU) process, approximating the steady-state distribution under each intervention induced by the OU process by solving the Lyapunov equation. Despite the novelty in methodology, Bicycle can handle only a hundred or so genes.

Key Limitations. Despite recent improvements to network inference, causal graphical methods remain difficult to scale and lack the expressivity to model cellular dynamics and regulatory cycles. Existing neural ODE-based methods (Hossain et al. [2024] and Jackson et al. [2023]) learn GRNs from a single experimental environment and cannot handle multiple genetic perturbations. PerturbODE combines causal structure learning and trajectory inference into a realistic and scalable framework that accurately captures cellular dynamics and infers the underlying GRN from thousands of perturbations.

3 Methods

Let $\mathcal{I} = \{I_0, I_1, \dots, I_K\}$ represent a set of $K + 1$ intervention regimes, with I_0 denoting the control regime (no intervention). The training dataset $\mathcal{D} = \{Y^{(r)}\}_{r=0}^K$ is a family of empirical distributions in the gene expression space, each corresponding to an intervention regime. $Y^{(r)} \in \mathbb{R}^{n_r \times d}$ represents the d -dimensional gene expression measurements of n_r cells under the intervention regime I_r . $Y^{(0)}$, the gene expression under the control regime, is used as the unperturbed initial state from which we integrate our neural ODE function f_r to predict the perturbation effect and final gene expression state under a given intervention.

3.1 Neural ODE formulation for over-expression with shift intervention

For any cell subject under intervention $I_r \in \mathcal{I} \setminus \{I_0\}$, its cellular dynamics are described by the ODE,

$$\frac{\partial y^{(r)}(t)}{\partial t} = f_r(y^{(r)}(t)) = A\sigma(\alpha \circ (By^{(r)}(t) - \beta)) + \sum_{j \in I_r} s_j \cdot \delta_j - Wy^{(r)}(t), \quad (1)$$

where $y^{(r)}(t) \in \mathbb{R}^d$ represents the expression vector at time t for a cell under intervention I_r .

This system encapsulates the interaction between genes through a Multi-Layer Perceptron (MLP) with a single hidden layer. Each neuron in the hidden layer is analogous to a gene module encapsulating co-regulated genes or biological pathways as outlined in Segal et al. [2005]. Module-based regulatory network structures have been established in prior literature. A well-characterized example is the regulatory circuit of *E. coli*'s flagella production [Macnab, 2003, Alon, 2006]. In Appendix A.14, we illustrate how this structure could be represented as a two-layer MLP.

The matrix $B \in \mathbb{R}^{l \times d}$ represents a linear transformation from d -dimensional gene expression $y^{(r)}(t)$ to a l -dimensional latent (“module”) space. B_{jm} is the signed effect of j -th gene’s expression on the m -th module.

The gene module signals are then nonlinearly transformed after shift and scaling through the non-linear activation function $\sigma(\cdot) : \mathbb{R}^l \rightarrow \mathbb{R}^l$. We use the logistic sigmoid function for gene module activation $\sigma(\cdot)$ due to its equivalence (when modeling log expression) to the Hill function, which, following basic chemistry principles, represents the effect of TF concentration on target gene transcription rate [Alon, 2006]. The vector $\beta \in \mathbb{R}^l$ is a strictly positive bias that shifts the activation threshold of the function σ in each module. The vector $\alpha \in \mathbb{R}^l$ is a scaling factor that modulates the rate of activation through a Hadamard (i.e., element-wise) product (\circ) with the gene modules.

The module activations regulate downstream genes by combining linearly with those from other modules. The matrix $A \in \mathbb{R}^{d \times l}$ maps the l -dimensional latent vector back to the d -dimensional gene expression space. A_{mj} represents the influence of the m -th module on the transcription rate of the j -th gene.

The interaction between genes mediated by modules encodes our estimate of the GRN matrix, $\mathbf{G} = A \text{diag}(\alpha)B$. Conveniently, working with the lower-dimensional module space reduces our task from learning the full gene-to-gene matrix of size $d \times d$ (i.e., d^2 parameters) to learning two factorized graphs of size $d \times l$ (i.e. $2dl$ parameters).

The matrix $W \in \mathbb{R}^{d \times d}$ is diagonal with strictly positive entries such that $W_{ii} > 0$ is the decay rate for gene i . The decay component $-W y^{(r)}(t)$ represents cellular RNA levels decreasing over time due to molecular decay and concentration dilution as cells grow and divide. Decay not only accurately models the regulatory biology but also encourages stability in the ODE system to prevent extreme levels of gene expression by creating a trapping region.

Interventions on the system are captured by the shift term $\delta_j = \mathbf{e}_j \in \mathbb{R}^d$, a standard basis vector corresponding to the induced over-expression of gene j (which in our case is a TF). The vector \mathbf{e}_j encodes a 1 in the j^{th} entry and 0 in all other entries, allowing variable dynamics between cells with overexpression of different TFs. The scaling term $s = (s_1, s_2, \dots, s_d)^\top$ specifies the strength of each intervention on each gene. Importantly, each entry in s is unique to a given intervention, while all other learned model parameters (A , B , W , α , and β) are shared between all interventions.

3.2 Neural ODE formulation with perfect intervention

We adapt PerturbODE to model perfect interventions. Gene knockout or overexpression (CRISPR-a) under perfect intervention is modeled by removing the intervened genes’ dependencies on parent nodes. In a system subject to a set I_r of perfect interventions, the corresponding ODE is,

$$\frac{\partial y^{(r)}}{\partial t} = M_r A \sigma(\alpha \circ (B y^{(r)}(t) - \beta)) + \sum_{j \in I_r} s_j \cdot \delta_j - W y^{(r)}(t) \quad (2)$$

where $M_r = \mathbf{I} - \sum_{j \in I_r} \text{diag}(\delta_j)$ is a masking matrix that removes the effect of other genes on the perturbed gene(s). For overexpression, $s_j > 0$ for all j , while for knockout we set $s_j = 0$ for all j .

3.3 Mapping dynamics to targets using optimal transport

We train f_r so that cells from $Y^{(0)}$ pushed forward through the dynamics fall close to $Y^{(r)}$. Specifically, we compute our target predictions $\widehat{Y}^{(r)}$ by numerically solving the ODE integration for each

cell in the initial distribution,

$$\begin{aligned}\hat{Y}^{(r)} &= [\phi_T^r(y_1^{(0)}), \dots, \phi_T^r(y_{n_r}^{(0)})]^\top \\ \phi_T^r(y_j^{(0)}) &= y_j^{(0)} + \int_0^T f_r(y_j^{(r)}(t)) dt\end{aligned}\tag{3}$$

where j indexes cells in $Y^{(0)}$ and ϕ_T^r is the flow map of the ODE under intervention I_r mapping initial cell state $y_j^{(0)}$ to its position at time T .

Given the lack of one-to-one correspondence between cells in the initial distribution $Y^{(0)}$ and the samples in the target distributions, we assess the quality of our predictions by measuring the Wasserstein-2 distance between observed distribution $Y^{(r)}$ and predicted distribution $\hat{Y}^{(r)}$,

$$W_2(X, \hat{X}) = \left(\min_{\Gamma \sim \Pi(X, \hat{X})} \sum_{x, y} \|X_x - \hat{X}_y\|_2^2 \Gamma_{xy} \right)^{1/2}, \tag{4}$$

where Π represents the set of all optimal transport plans between each sample from data distributions X and \hat{X} , and Γ represents the minimal-cost transport plan used to measure the dissimilarity between X and \hat{X} . The total loss function is defined as the average W_2 between $\hat{Y}^{(r)}$ and $Y^{(r)}$ for all perturbations in \mathcal{I} in addition to the L_1 norm of B to encourage sparsity,

$$\mathcal{L}(\theta) = W_2(Y^{(r)}, \hat{Y}^{(r)}) + \lambda|B|_1. \tag{5}$$

During training, for each intervention I_r , we push the control samples $Y^{(0)}$ through the map ϕ_T^r to obtain the predicted targets $\hat{Y}^{(r)}$. We backpropagate through the loss and ODE solver to obtain gradients for all parameters. L_1 penalty is enforced only on B because the network motif of a multiple-input feedforward loop is significantly less common than that of a multiple-output feedforward loop in known GRNs of yeast and E. coli [Kashtan et al., 2004]. Training details and loss convergence plots can be found in Appendix A.9.

3.4 Diffusion-based regularization of neural dynamics

PerturbODE can optionally augment the primary training objective by using diffused target samples as alternative initial states. This additional regularization encodes our prior expectation that the final cell states should be locally stable, helping to form a local contraction map that implies a locally stable fixed point, as ensured by the Contraction Mapping Theorem [Hunter and Nachtergael, 2000]. Interestingly, the stable fixed points establish the theoretical equivalence between PerturbODE and a deterministic structural causal model (SCM) Mooij et al. [2013], Schölkopf et al. [2021].

The augmentation involves diffusing $Y^{(r)}$ using Brownian motion with a time step Δt to generate diffused targets $Y_{\text{diff}}^{(r)}$. During a reduced time span $t \leq T$, $Y_{\text{diff}}^{(r)}$ is pushed forward through $\phi_t^{(r)}$ to obtain the predicted targets $\hat{Y}_{\text{diff}}^{(r)}$, and we backpropagate against the augmented loss $\tilde{\mathcal{L}} = W_2(\hat{Y}_{\text{diff}}^{(r)}, Y^{(r)}) + \lambda|B|_1$. During training, we alternate between using control samples $Y^{(0)}$ and diffused targets $Y_{\text{diff}}^{(r)}$ for each intervention. Information on diffusion training hyperparameters can be found in Appendix A.3.1.

4 Results

We compare PerturbODE to the causal graph discovery methods DCDFG [Lopez et al., 2022], DCDI [Brouillard et al., 2020], NO-TEARS [Zheng et al., 2018], NO-TEARS-LR [Fang et al., 2023], and Bicycle [Rohbeck et al., 2024] on both simulated and large-scale perturbational scRNA-seq datasets. These methods are most appropriate for comparison as they are equipped to learn a causal GRN from multiple interventions without requiring multiple time points or pseudotime.

4.1 GRN inference on simulated datasets

SERGIO [Dibaeinia and Sinha, 2020] and BoolODE [Pratapa et al., 2020] simulate single-cell gene expression data by sampling from a stochastic differential equation (SDE) parameterized by a

user-provided ground-truth GRN. SERGIO simulates mature cells of any cell type in steady state or stem cells differentiating to multiple fates. By requiring an acyclic input GRN, cells are initialized at the mean of the steady-state distribution. BoolODE uses manually constructed cyclic GRNs with tens of genes that lead to convergent trajectories from predefined initial conditions.

We extend SERGIO and BoolODE to simulate gene expression with overexpression perturbations. We implement interventions by masking the transcription induced by TF interactions (analogously to M_r in Equation 2) of the intervened genes and adding a scalar to the intervened gene's transcription rate. We select an experimentally curated GRN identified for yeast cells with dimension 400 as the input to SERGIO for simulation [Liu et al., 2015]. The output synthetic dataset from SERGIO consists of 10,100 cells generated from 100 intervention schemes, each targeting 5 genes and one non-intervention (control) scheme. Each regime contains measurements of 100 cells. To evaluate the models against a diverse range of networks, we simulate ten random DAGs with dimension 100 in the same manner. We used a bifurcating convergent synthetic cyclic network to simulate data using BoolODE. We compare the models' performance using the area under the precision-recall curve (AUPRC). Other metrics exhibited strong sensitivity to user-selected threshold values for edge classification, making them unreliable for benchmarking. Details on BoolODE, SERGIO, and the effects of thresholding and varying the number of modules are presented in Appendix A.13, A.12, and A.6, respectively.

In Figure 2, we evaluated model performance on data simulated using BoolODE with 10 genes. PerturbODE outperforms Bicycle, DCDFG, DCDI, and NO-TEARS-LR, while performing worse than NO-TEARS and GENIE3 in a low-dimensional setting.

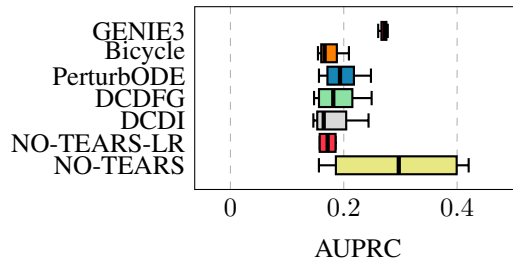


Figure 2: Performance metrics on data simulated from a synthetic GRN (10 genes) using BoolODE assuming perfect over-expression (CRISPR-a). 5 runs are conducted for the synthetic GRN.

When scaling to simulations with 100 genes across 10 randomly generated GRNs (Figure 3a), PerturbODE and Bicycle yield comparable performance, with DCDI and GENIE3 marginally outperforming both. DCDFG trails slightly behind PerturbODE and Bicycle, while NO-TEARS and NO-TEARS-LR show significantly reduced performance, highlighting their limitations in higher-dimensional regimes.

For simulations based on a known yeast GRN involving 400 genes (Figure 3b), PerturbODE exhibits greater comparative performance. Bicycle could not be assessed due to memory limitations, underscoring its lack of scalability. While DCDI achieves the highest performance in this setting, PerturbODE surpasses DCDFG, GENIE3, NO-TEARS, and NO-TEARS-LR. Notably, as the number of causal variables increases, other methods begin to break down due to memory constraints (Bicycle) or numerical instability during optimization (DCDI). In contrast, PerturbODE remains robust and consistent in its performance, which becomes more apparent in benchmarks on the TF Atlas dataset.

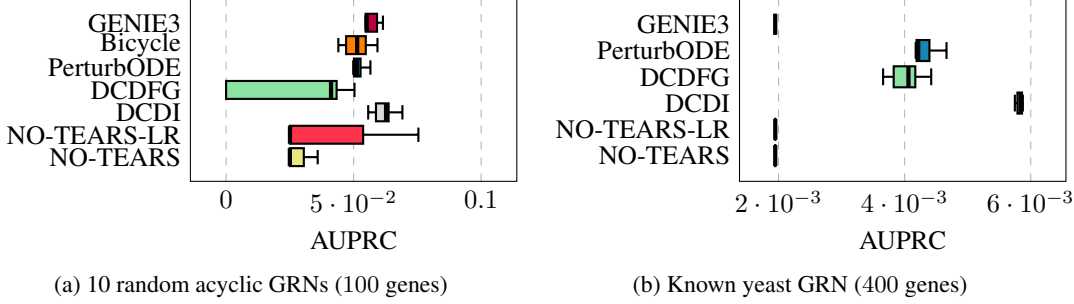


Figure 3: Performance metrics on SERGIO-simulated data assuming perfect over-expression (CRISPR-a). 5 runs are conducted for the yeast GRN.

4.2 GRN inference on the TF Atlas

We trained PerturbODE on the TF Atlas to evaluate its performance on a large-scale real dataset. The TF Atlas overexpresses TFs and uses scRNA-seq to measure cell states after 7 days of perturbation [Joung et al., 2023]. As this dataset maps the interventional effects of TF overexpression, PerturbODE’s inferred GRNs can uncover TF-to-TF interactions and higher-level network structure through TF modules.

We used the control samples (mCherry) as the initial gene expression values for solving the neural ODE (Equation 1). Using the inferred neural ODE trajectories, we compared the predicted final cell states with ground-truth gene expression measured after 7 days of TF overexpression. To evaluate the model’s ability to recover GRNs, we used three well-studied and experimentally validated human GRNs derived from extensive RNA-seq and ATAC-seq measurements generated as part of the TF Atlas study (see Appendix A.10). Since the GRNs contain only positive directed edges, our ground truth is restricted to true positives and false negatives. Consequently, we only computed recall scores for edge detection on the three TF-Atlas human GRNs (Appendix A.6.1). To assess statistical significance of the model predictions, we compared the inferred GRNs with random matrices and computed a p -value (Appendix A.4).

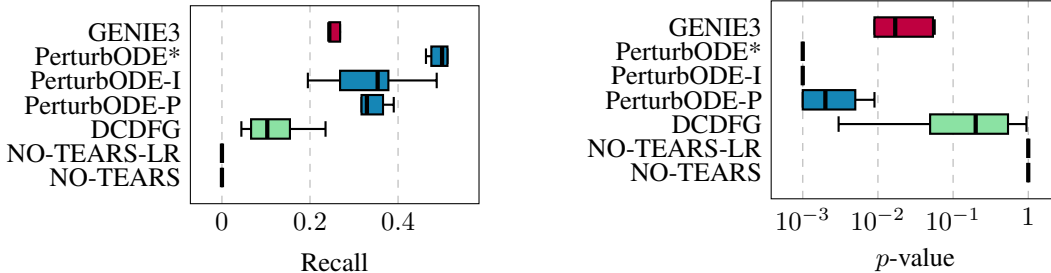


Figure 4: GRN inference performance on the TF Atlas dataset (812 genes), evaluated against three experimentally validated human GRNs.

We benchmark PerturbODE against GENIE3, DCDFG, NO-TEARS, and NO-TEARS-LR by training on the union of the top 500 highly variable genes and the experimentally intervened genes that are differentially expressed, resulting in a total of 812 genes. Due to memory constraints and numerical instability, Bicycle and DCDI fail to scale to datasets of this size and are therefore excluded from comparison. We evaluate PerturbODE under both perfect (P) and imperfect (I) intervention. PerturbODE* refers to the model with tunable overexpression strength s for each gene (Equation 1).

PerturbODE achieves the highest recall and statistical significance on the TF Atlas human reference GRNs. In Figure 4, PerturbODE* with imperfect intervention significantly outperforms DCDFG, NO-TEARS, and NO-TEARS-LR in recall scores with higher statistical significance. While GENIE3 performs comparably, it lags behind PerturbODE overall. In Figure 6, we further assess the model’s predictions across different sparsity levels by varying the thresholds for edge classification.

PerturbODE* with imperfect interventions outperforms all other methods at most thresholds, with only GENIE3 marginally outperforming PerturbODE* at low sparsity levels.

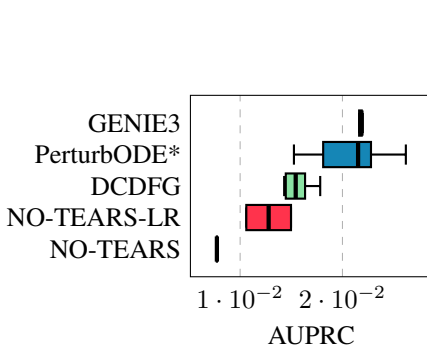


Figure 5: GRN inference on TF Atlas dataset (812 genes), validated with ChIP-Atlas.

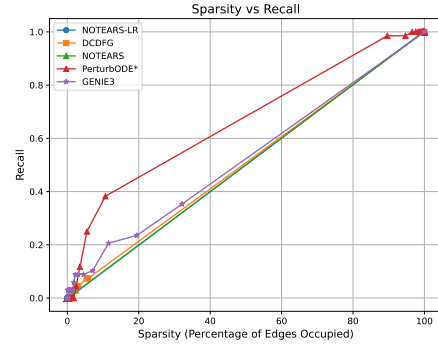


Figure 6: Recall across models on TF Atlas at various sparsity levels.

PerturbODE achieves the highest AUPRC on reference GRNs from ChIP-Atlas. In Figure 5, we further validate GRN predictions using a reference network with 223 genes derived from ChIP-Seq data provided by ChIP-Atlas [Zou et al., 2024]. Unlike our previous benchmark, this network includes both true positive and true negative edges, allowing us to assess performance using the AUPRC metric. Across all tested models, PerturbODE* achieves the highest AUPRC, indicating superior performance in distinguishing true regulatory interactions from non-interactions.

Table 1: Sparsity (%) and False Discovery Rate (FDR %) across three threshold settings (Low, Medium, High) on reference GRN derived from ChIP-Atlas.

Method	Low		Medium		High	
	Sparsity	FDR	Sparsity	FDR	Sparsity	FDR
PerturbODE	31.0	55.4	8.1	52.5	3.8	50.2
GENIE3	33.5	54.1	8.2	54.1	3.9	55.0
DCDFG	38.7	58.8	8.3	58.8	3.7	58.7
NO-TEARS	N/A	N/A	N/A	N/A	0.2	N/A
NO-TEARS-LR	N/A	N/A	N/A	N/A	0.4	N/A

In Table 1, we compare the False Discovery Rate (FDR) of each method at three threshold settings using the ChIP-Atlas reference GRN. Compared to GENIE3, PerturbODE has a lower FDR at medium and high threshold levels, while its FDR is slightly higher at the low threshold level. PerturbODE comfortably outperforms DCDFG at all sparsity levels. The FDRs of NO-TEARS and NO-TEARS-LR could not be obtained as they predict close to empty graphs with their predicted edges not being in the ChIP-Atlas.

PerturbODE uncovers biologically meaningful gene network structure from its latent GRN modules. We directly interpret PerturbODE’s gene modules trained on the TF Atlas dataset. Each module represents a set of gene-to-gene interactions derived from the model’s A and B matrices (Equation 1), capturing upstream regulators and downstream targets. The most statistically significant modules recover known developmental GRNs, including those involved in anterior-posterior axis specification and trophoblast/vascular lineage induction. Our gene set enrichment analysis (GSEA) reveals a strong alignment of the modules with pathways involved in angiogenesis, fluid stress response, and early embryonic development. See Appendix A.11.2 for the full analysis.

4.3 Predicting the effects of held-out interventions on gene expression

Predicting the effects of unseen interventions is a particularly challenging task. Here, we randomly select ten overexpressed TFs to be held out simultaneously during training. Note that their expression

levels of these genes are observed, but their perturbations are not trained on. For this task, we compare PerturbODE with two linear SCMs (NO-TEARS and NO-TEARS-LR), a simple linear baseline introduced by Ahlmann-Eltze et al. [2024], the GNN-based method GEARS [Roohani et al., 2024], and the single-cell foundation model scGPT [Cui et al., 2024]. DCDFG cannot sample cells given a learned GRN, and DCDI does not scale to this data. For linear SCMs, overexpression is implemented as an imperfect shift intervention by adding a bias to the mean of the distribution modeling the intervened nodes (see Appendix A.5).

We evaluate predictive performance through W_2 distance and cell-type distance between the predicted and true distributions, and visual inspection through low-dimensional UMAP embeddings. W_2 distance is calculated between the full distributions of the predicted and observed gene expressions. The cell-type distance measures how closely our predictions align with the ground truth in estimating the cell type induced by each perturbation (see Appendix A.16 for details). Figure 7 presents UMAP visualizations of model predictions, with further examples in Appendix A.8.2.

Table 2: Predictive performance on held-out interventions in TF-Atlas.

Method	W_2	Cell-Type Dist.	TF	PerturbODE	GEARS	scGPT	NO-TEARS-LR	Linear	NO-TEARS
PerturbODE	84 ± 88	0.86 ± 0.39	ZNF69	85.4	63.3	88.1	106.0	110.9	164.9
GEARS	65 ± 7.3	0.89 ± 0.20	SETDB1	261.9	60.5	82.9	97.2	114.1	157.9
scGPT	91 ± 14	0.90 ± 0.23	POU2AF1	300.8	59.6	95.9	105.5	113.9	163.1
NO-TEARS-LR	105 ± 9	1.08 ± 0.26	ZBTB37	69.4	68.6	91.0	107.1	114.1	165.9
Linear Baseline	113 ± 11	0.88 ± 0.20	IRF3	73.6	71.8	77.0	111.2	118.6	170.1
NO-TEARS	396 ± 9	1.00 ± 0.19	IDI	79.6	69.2	82.9	109.7	114.7	168.7
			TEAD1	244.6	60.7	107.1	106.1	102.5	163.5
			ASCL1	94.1	84.2	116.4	134.8	144.2	192.7
			KCNIP4	82.7	N/A	63.4	104.7	112.6	163.7
			MSX2	66.7	65.1	91.2	103.7	110.2	164.6

(a) Predictive performance on 10 held-out interventions (median \pm std).

(b) Test errors (W_2) for TF over-expressions across models.

PerturbODE significantly outperforms all linear methods in terms of W_2 distance and cell-type distance with held-out interventions (Table 2a and Table 2b). However, when the model mispredicts, the associated prediction errors tend to be larger. PerturbODE outperforms scGPT in terms of W_2 distance and cell type distance. As illustrated in the UMAP visualization, scGPT fails to meaningfully encode perturbation signals—its predictions are dispersed across both the control group and test data.

PerturbODE performs competitively with GEARS but falls short in terms of W_2 distance. Both methods achieve comparable performance in cell type classification, with PerturbODE showing a slight advantage. However, it is worth noting that GEARS integrates a knowledge graph from Gene Ontology (GO) annotations as an additional biological prior to aid its predictions. Augmenting our gene representations is a promising direction for improving PerturbODE in future work.

For additional context on the scale of W_2 , the average gene expression of the training data has a median W_2 distance of 107 ± 8 from the test data distributions.

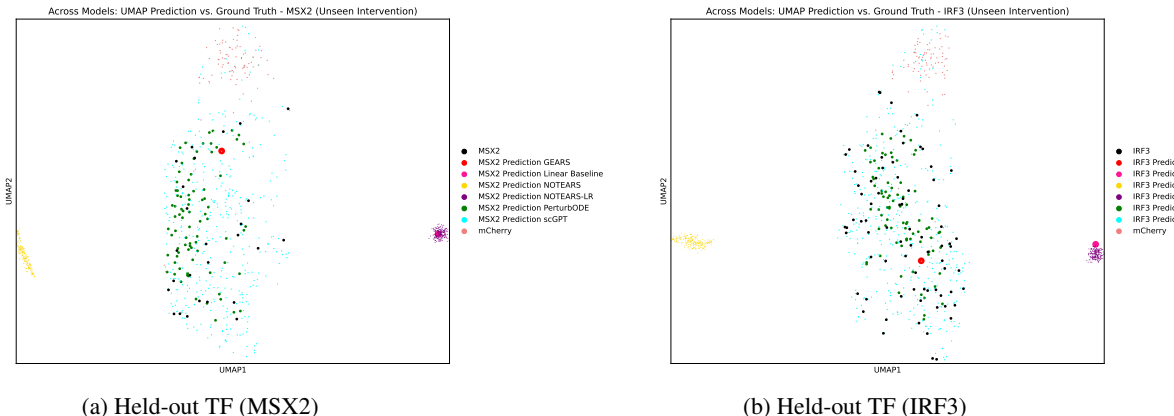


Figure 7: UMAP projections of cell embeddings: predictions for two held-out TFs—MSX2 and IRF3—found only in the test set.

5 Discussion

The question of identifiability of the ODE parameters is somewhat delicate. We assume the true underlying dynamics to be a deterministic system, inducing a family of stable fixed points, each corresponding to a perturbation. Authors [2025] has proved identifiability in a low noise regime for an SDE extension of our model. It in principle follows for the noiseless ODE case that the parameters are identifiable (up to permutations) when the number of interventions exceeds the gene dimension. Future work could explore a rigorous proof for this case.

6 Conclusion

PerturbODE is a highly scalable and biologically grounded causal approach to inferring GRNs from high-throughput genetic perturbation data. Building on the success of dynamical systems in modeling gene regulation and single-cell trajectories, our method presents a compelling alternative to traditional SCMs for causal discovery. At its core, PerturbODE employs a two-layer neural network with sigmoid activation that mirrors cellular regulatory processes. The framework achieves both strong predictive performance and biological interpretability of the learned parameters. In benchmarks, PerturbODE outperforms existing scalable methods on SERGIO-simulated datasets and large-scale single-cell experiments, while performing competitively against state-of-the-art but less scalable methods like DCDI. PerturbODE can also accurately predict cellular responses to previously unseen perturbations. Future work will incorporate ATAC-seq and ChIP-seq data to narrow down the candidate regulatory targets and mitigate false discoveries. Furthermore, training PerturbODE on scRNA-seq datasets with multiple time points will help the model better distinguish direct and indirect causal effects between genes [Davidson, 2006, p.133-134].

7 Acknowledgment

This work was made possible by support from the MacMillan Family and the MacMillan Center for the Study of the Non-Coding Cancer Genome at the New York Genome Center.

References

Constantin Ahlmann-Eltze, Wolfgang Huber, and Simon Anders. Deep learning-based predictions of gene perturbation effects do not yet outperform simple linear methods. *bioRxiv*, 2024. doi: 10.1101/2024.09.16.613342. URL <https://doi.org/10.1101/2024.09.16.613342>. Preprint.

Uri Alon. *An Introduction to Systems Biology: Design Principles of Biological Circuits*. CRC Press Taylor & Francis Group, A Chapman & Hall Book, 2006.

Anonymous Authors. Towards identifiability of interventional stochastic differential equations. 2025.

Philippe Brouillard, Sébastien Lachapelle, Alexandre Lacoste, Simon Lacoste-Julien, and Alexandre Drouin. Differentiable causal discovery from interventional data. In *Proceedings of the 34th Conference on Neural Information Processing Systems (NeurIPS 2020)*, Vancouver, Canada, 2020.

Ricky T. Q. Chen. torchdiffeq, June 2021. URL <https://github.com/rtqichen/torchdiffeq>.

Ricky T. Q. Chen, Yulia Rubanova, Jesse Bettencourt, and David K. Duvenaud. Neural ordinary differential equations. In *Advances in Neural Information Processing Systems 31 (NeurIPS 2018)*, pages 6571–6583, 2018.

Haotian Cui, Chloe Wang, Hassaan Maan, Kuan Pang, Fengning Luo, Nan Duan, and Bo Wang. scgpt: toward building a foundation model for single-cell multi-omics using generative ai. *Nature Methods*, 21(8):1470–1480, 2024. doi: 10.1038/s41592-024-02201-0. URL <https://doi.org/10.1038/s41592-024-02201-0>.

Eric H. Davidson. *The Regulatory Genome: Gene Regulatory Networks in Development and Evolution*. Academic Press, 2006. doi: 10.1016/B978-0-12-088563-3.X5018-4.

E. Dejana, A. Taddei, and A.M. Randi. Foxs and ets in the transcriptional regulation of endothelial cell differentiation and angiogenesis. *Biochim. Biophys. Acta*, 1775:298–312, 2007. doi: 10.1016/j.bbcan.2007.05.003. URL <https://doi.org/10.1016/j.bbcan.2007.05.003>.

Payam Dibaeinia and Saurabh Sinha. Sergio: A single-cell expression simulator guided by gene regulatory networks. *Cell Systems*, 11(3):252–271.e11, 2020. ISSN 2405-4712. doi: <https://doi.org/10.1016/j.cels.2020.08.003>. URL <https://www.sciencedirect.com/science/article/pii/S2405471220302878>.

Atray Dixit, Oren Parnas, Biyu Li, Jenny Chen, Charles P Fulco, Livnat Jerby-Arnon, Nemanja D Marjanovic, Danielle Dionne, Tyler Burks, Rakta Raychowdhury, Britt Adamson, Thomas M Norman, Eric S Lander, Jonathan S Weissman, Nir Friedman, and Aviv Regev. Perturb-seq: Dissecting molecular circuits with scalable single-cell RNA profiling of pooled genetic screens. *Cell*, 167(7):1853–1866.e17, December 2016. URL <https://pmc.ncbi.nlm.nih.gov/articles/PMC5181115/>.

Weinan E, Tiejun Li, and Eric Vanden-Eijnden. *Applied Stochastic Analysis*, volume 199 of *Graduate Studies in Mathematics*. American Mathematical Society, 2019.

Zhuangyan Fang, Shengyu Zhu, Jiji Zhang, Yue Liu, Zhitang Chen, and Yangbo He. On low rank directed acyclic graphs and causal structure learning. *arXiv preprint arXiv:2006.05691*, cs.LG, 2023. <https://arxiv.org/abs/2006.05691v2>.

Zhuangyan Fang, Shengyu Zhu, Jiji Zhang, Yue Liu, Zhitang Chen, and Yangbo He. On low-rank directed acyclic graphs and causal structure learning. *IEEE Transactions on Neural Networks and Learning Systems*, 35(4):4924–4937, 2024. doi: 10.1109/TNNLS.2023.3273353.

Jean Feydy, Thibault Séjourné, François-Xavier Vialard, Shun-ichi Amari, Alain Trouve, and Gabriel Peyré. Interpolating between optimal transport and mmd using sinkhorn divergences. In *The 22nd International Conference on Artificial Intelligence and Statistics*, pages 2681–2690, 2019.

Gennady Gorin and Lior Pachter. Length biases in single-cell rna sequencing of pre-mrna. *Biophysical Reports*, 3(1):100097, 2023. doi: 10.1016/j.bpr.2022.100097. URL <https://doi.org/10.1016/j.bpr.2022.100097>.

Intekhab Hossain, Viola Fanfani, Jonas Fischer, John Quackenbush, and Rebekka Burkholz. Biologically informed neuralodes for genome-wide regulatory dynamics. *Preprint*, 2024. Available at [source if applicable].

John K. Hunter and Bruno Nachtergael. *Applied Analysis*. University of California at Davis, Department of Mathematics, University of California at Davis, 2000.

Vân Anh Huynh-Thu, Alexandre Irrthum, Louis Wehenkel, and Pierre Geurts. Inferring regulatory networks from expression data using tree-based methods. *PLoS ONE*, 5(9):e12776, 2010. doi: 10.1371/journal.pone.0012776.

Christopher A. Jackson, Maggie Beheler-Amass, Andreas Tjärnberg, Ina Suresh, Angela Shang mei Hickey, Richard Bonneau, and David Gresham. Simultaneous estimation of gene regulatory network structure and rna kinetics from single cell gene expression. *bioRxiv*, 2023. doi: 10.1101/2023.09.21.558277. URL <https://doi.org/10.1101/2023.09.21.558277>.

Julia Joung, Sai Ma, Tristan Tay, Kathryn R. Geiger-Schuller, Paul C. Kirchgatterer, Vanessa K. Verdine, Baolin Guo, Mario A. Arias-Garcia, William E. Allen, Ankita Singh, Olena Kuksenko, Omar O. Abudayyeh, Jonathan S. Gootenberg, Zhanyan Fu, Rhiannon K. Macrae, Jason D. Buenrostro, Aviv Regev, and Feng Zhang. A transcription factor atlas of directed differentiation. *Cell*, 186:209–229, 2023. doi: 10.1016/j.cell.2022.11.026. URL <https://doi.org/10.1016/j.cell.2022.11.026>.

Shiraz Kalir and Uri Alon. Using a quantitative blueprint to reprogram the dynamics of the flagella gene network. *Cell*, 117(6):713–720, 2004. doi: 10.1016/j.cell.2004.05.010.

N. Kashtan, S. Itzkovitz, R. Milo, and U. Alon. Topological generalizations of network motifs. *Physical Review E*, 70(3):031909, 2004. doi: 10.1103/PhysRevE.70.031909.

C. Krendl, D. Shaposhnikov, V. Rishko, C. Ori, C. Ziegenhain, S. Sass, L. Simon, N.S. Müller, T. Straub, K.E. Brooks, et al. Gata2/3-tfap2a/c transcription factor network couples human pluripotent stem cell differentiation to trophectoderm with repression of pluripotency. *Proc. Natl. Acad. Sci. USA*, 114:E9579–E9588, 2017. doi: 10.1073/pnas.1708341114. URL <https://doi.org/10.1073/pnas.1708341114>.

Zhi-Ping Liu, Canglin Wu, Hongyu Miao, and Hui Wu. Regnetwork: an integrated database of transcriptional and post-transcriptional regulatory networks in human and mouse. *Database*, 2015: bav095, 2015. doi: 10.1093/database/bav095. URL <http://www.regnetworkweb.org>.

Romain Lopez. Dcdfg: Large-scale differentiable causal discovery of factor graphs. <https://github.com/Genentech/dcdfg>, 2024. Accessed: 2024-09-19.

Romain Lopez, Jan-Christian Hütter, Jonathan K. Pritchard, and Aviv Regev. Large-scale differentiable causal discovery of factor graphs. *36th Conference on Neural Information Processing Systems (NeurIPS 2022)*, October 2022.

Robert M. Macnab. How bacteria assemble flagella. *Annual Review of Microbiology*, 57:77–100, 2003. doi: 10.1146/annurev.micro.57.030502.090832. First published online as a Review in Advance on May 1, 2003.

Joris M. Mooij, Dominik Janzing, and Bernhard Schölkopf. From ordinary differential equations to structural causal models: The deterministic case. *arXiv preprint arXiv:1312.4180*, 2013.

Roel Neijts, Shilu Amin, Carina van Rooijen, and Jacqueline Deschamps. Cdx is crucial for the timing mechanism driving colinear hox activation and defines a trunk segment in the hox cluster topology. *Developmental Biology*, 422(2):146–154, 2017.

Aditya Pratapa, Amogh P. Jalihal, Jeffrey N. Law, Aditya Bharadwaj, and T. M. Murali. Benchmarking algorithms for gene regulatory network inference from single-cell transcriptomic data. *Nature Methods*, 17:147–154, 2020. doi: 10.1038/s41592-019-0690-6. URL <https://doi.org/10.1038/s41592-019-0690-6>.

Martin Rohbeck, Brian Clarke, Katharina Mikulik, Alexandra Pettet, Oliver Stegle, and Kai Ueltzhöfer. Bicycle: Intervention-based causal discovery with cycles. In *Proceedings of Machine Learning Research*, volume 236, pages 209–242. 3rd Conference on Causal Learning and Reasoning, 2024.

Yusuf Roohani, Kexin Huang, and Jure Leskovec. Predicting transcriptional outcomes of novel multigene perturbations with gears. *Nature Biotechnology*, 42(6):927–935, 2024. doi: 10.1038/s41587-023-01905-6. URL <https://doi.org/10.1038/s41587-023-01905-6>.

Bernhard Schölkopf, Francesco Locatello, Stefan Bauer, Nan Rosemary Ke, Nal Kalchbrenner, Anirudh Goyal, and Yoshua Bengio. Towards causal representation learning. *arXiv preprint arXiv:2102.11107*, 2021.

Eran Segal, Dana Pe'er, Aviv Regev, Daphne Koller, and Nir Friedman. Learning module networks. *Journal of Machine Learning Research*, 6:557–588, 2005.

Y. Setty, A.E. Mayo, M.G. Surette, and U. Alon. Detailed map of a cis-regulatory input function. *Proceedings of the National Academy of Sciences*, 100(13):7702–7707, 2003.

Alejandro Tejada-Lapuerta, Paul Bertin, Stefan Bauer, Hananeh Aliee, Yoshua Bengio, and Fabian J. Theis. Causal machine learning for single-cell genomics. *Cell Systems*, 2023. doi: 10.1016/j.cels.2023.08.014. URL <https://doi.org/10.1016/j.cels.2023.08.014>.

Xun Zheng, Bryon Aragam, Pradeep Ravikumar, and Eric P. Xing. Dags with no tears: Continuous optimization for structure learning. *Carnegie Mellon University*, November 2018. Available online at <https://github.com/xunzheng/notears>.

Zhaonan Zou, Tazro Ohta, and Shinya Oki. ChIP-Atlas 3.0: a data-mining suite to explore chromosome architecture together with large-scale regulome data. *Nucleic Acids Research*, 52(W1):W45–W53, July 2024. doi: 10.1093/nar/gkae358. URL <https://doi.org/10.1093/nar/gkae358>.

A Appendix

A.1 Broader Impacts

This work aims to accelerate biomedical research by helping to identify key genetic regulators and potential intervention targets for drug development. Any network or cell state predictions made using our method must be validated in the wet lab before using these results in downstream scientific or clinical decisions. In general, experimental validation will promote the responsible use of machine learning-based prediction models in biology.

A.2 Preprocessing

The scRNA-seq gene expression matrix is normalized per cell by 10^4 and $\log(1 + X)$ transformed. The total gene expression vector comprises RNA counts for N genes consisting of all the TF over-expression genes j and the top $k = 500$ highly variable genes.

For each TF gene j , we perform a Mann-Whitney U test on differential gene expression of TF j between the unperturbed control samples in X_0 and over-expressed samples in X_j consisting of n_j cells. The returned p-value p_j from the U test determines whether over-expression of the targeted TF gene j is sufficiently induced in the experiments. The dataset is then filtered based on the criteria $\mathcal{D} = \{X_j \mid p_j < 0.1 \text{ and } n_j \geq 10, \forall j \in \{1, 2, \dots, M\}\}$.

Over-expression distributions of the genes encoding the GRNs of interest are added to the training and validation dataset. In addition, when training for GRN inference only without trajectory prediction, distributions of TF over-expression encoded by the marker genes of the cell types or the developmental role targeted by the genes in the GRNs are included in the joint train, test, and validation dataset.

We design a train-test split based on TF over-expression genes to select $\mathcal{D}_{\text{train, val}}$ and $\mathcal{D}_{\text{test}}$. For each $X_j \in \mathcal{D}_{\text{train, val}}$ where $n_j \geq 100$, we apply a 80% to 20% training-validation split of the over-expression samples. If $n_j < 100$, we would use all the samples in X_j for $\mathcal{D}_{\text{train}}$ due to an insufficient number of training samples.

Furthermore, we apply the `log1p` transformation to prevent negative predictions of gene expression and mitigate length biases in expression counts [Gorin and Pachter, 2023]. This transformation results in a substantial improvement in model performance.

A.3 Model Specifications

PerturbODE utilizes adaptive Runge-Kutta of order 5 of Dormand-Prince-Shampine which provides an exceptionally high order of accuracy and leverages its adaptive step size for efficient ODE solving. The adaptive step size also detects and handles a wide range of stiff ODEs. Differentiable numerical solution is computed via the adjoint method implemented in PyTorch by Chen [2021], available at <https://github.com/rtqichen/torchdiffeq>. The Sinkhorn-based W_2 distance is differentiable through the `GeomLoss` implementation in PyTorch [Feydy et al., 2019].

For the GRN inference baseline methods, the authors of DCDFG have implemented DCDI, DCDFG, NO-TEARS, and NO-TEARS-LR in the repository Lopez [2024], available at <https://github.com/Genentech/dcdfg>. Bicycle is implemented by Rohbeck et al. [2024] with code available at <https://github.com/PMBio/Bicycle>. GENIE3 is implemented by Huynh-Thu et al. [2010] with code available at <https://github.com/vahuynh/GENIE3>.

When benchmarking prediction of perturbation effects, we implemented the linear baseline of Ahlmann-Eltze et al. [2024] in numpy. GEARS is implemented by Roohani et al. [2024] at <https://github.com/snap-stanford/GEARS>, and scGPT is implemented by Cui et al. [2024] at <https://github.com/bowang-lab/scGPT>.

A.3.1 Hyperparameters

Spectral radius is used as the DAG constraint for DCDI, DCDFG, NO-TEARS, and NO-TEARS-LR. Notably, NO-TEARS and DCDI fail to run at dimensions higher than tens of variables with the trace exponential constraint. After hyperparameter-tuning, we set the optimizer learning rate to 0.001 and the regularization coefficient to 0.1. Other hyperparameters are set as default.

For Bicycle, the hyperparameters are chosen as following: learning rate = 0.001, gradient_clip_var = 0.001, scale_kl = 1, scale_spectral = 0, and scale_lyapunov = 0.1. We set the other hyper-parameters as default.

When running GENIE3, we set $n_trees = 1000$ after hyperparameter-tuning. Other hyper-parameters remained as default.

For GEARS, after hyperparameter-tuning, we found the optimal hyperparameter to be the following: learning rate = 0.0001, $hidden_size = 128$, and $epoch = 50$. Meanwhile, for scGPT, we found the optimal hyper-parameters to be the following: $embsize = 256$, $d_hid = 512$, $n_layers_cls = 5$, $lr = 0.003$, and $batch_size = 64$. The rest of hyper-parameters are set as default.

The number of modules is optimally set to 10 for NO-TEARS-LR and DCDFG. For PerturbODE, we set the number of modules to 100 for simulated data and 200 for TF Atlas. Details on performances across different number of modules in all models can be found in Figure 11.

As the number of modules increases, the model becomes closer to approximating the full graph. On the TF Atlas dataset, we demonstrate that the validation loss for PerturbODE decreases as the number of modules increases, plateauing after reaching 200 modules when training on TF Atlas (Fig. 8).

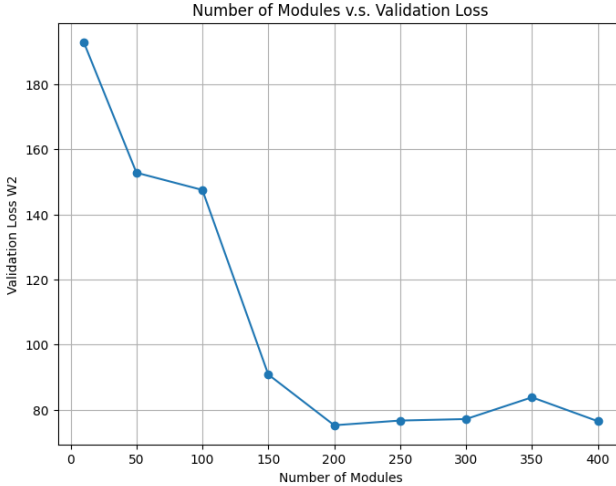


Figure 8: PerturbODE: number of modules v.s. validation loss in TF Atlas

On a separate note, PerturbODE uses 50 time steps for both diffused and non-diffused training when solving the ODE numerically. For diffused training, the time step duration t is set to 0.1, while for non-diffused training, it is set to 25. The lasso regularization coefficient, λ , is set to 0.001. When computing the W_2 distance through Sinkhorn’s algorithm, the coefficient for entropic regularization is set to 0.05. Δt for the Brownian motion used to generate diffused data is set to 0.3.

A.4 Comparison to Erdős-Rényi Random Graphs

We generate 10,000 random graphs with the same density as our inferred GRN to numerically simulate the test statistics under Erdős-Rényi random matrices. The p-value is calculated using the equation,

$$p\text{-value} = \frac{1 + \#\{\tau^* \geq \tau\}}{1 + \Pi} \quad (6)$$

where τ is the test statistic, Π indicates the total number of random graphs, and τ^* denotes the test statistics computed from each graph. The p-value quantifies how often a test statistic is observed (or a more extreme one) purely by chance.

When evaluating SERGIO simulated data, the test statistics used is the F1 score, whereas recall score is used for TF Atlas due to availability of only positive benchmark edges. To identify gene modules,

we use test statistics based on the count of incoming edges to the module and outgoing edges from the module that are consistent with known regulatory relationships. Further, to identify the network motif of negative auto-regulation, test statistics is the number of negative self-loops.

A.5 Sampling from Linear SCMs for TF Atlas

For a learned GRN represented by \mathbf{W} (ensured to be a DAG, or thresholded to enforce acyclicity), we sample from linear structural causal models (SCMs) using the following procedure. First, for each parent gene i (master regulator) in the GRN, if not over-expressed, its expression level X_i is sampled from a normal distribution, $X_i \sim \mathcal{N}(\mu, \sigma)$, where μ and σ represent the mean and standard deviation of gene expression levels across all genes and cells in the TF Atlas, respectively. If X_i is over-expressed, it is instead sampled from $X_i \sim \mathcal{N}(\mu_\gamma, \sigma_\gamma)$ where μ_γ and σ_γ are the mean and standard deviation of gene expression levels in over-expression genes across all over-expressed cells.

Downstream genes are realized in Equation 7:

$$\begin{aligned} X_i &= \sum_{X_j \in \text{pa}(X_i, \mathbf{W})} \mathbf{W}_{j,i} X_j && \text{if } X_i \text{ is not over-expressed,} \\ X_i &= \sum_{X_j \in \text{pa}(X_i, \mathbf{W})} \mathbf{W}_{j,i} X_j + \gamma_i, \quad \gamma_i \sim \mathcal{N}(\mu_\gamma - \mu, \sigma_{\Delta\gamma}) && \text{if } X_i \text{ is over-expressed,} \end{aligned} \quad (7)$$

where $\sigma_{\Delta\gamma}$ is the standard deviation of the differences between over-expressed genes and mean expression levels (average over genes) across all over-expressed cells. Further, $\text{pa}(X_i, \mathbf{W})$ denotes all the parent genes (regulators) of gene i in the GRN \mathbf{W} .

A.6 Additional Thresholded Result

A.6.1 Thresholds

The performance evaluation in the main body mainly looks at AUPRC as the choice of thresholds could affect evaluation drastically. For additional evaluations, here we apply thresholds ϵ to the predicted GRN matrices \mathbf{G} , where any edge with a weight below ϵ is set to 0 and any edge whose weight exceeds ϵ is set to 1.

As recommended by their authors, DCDFG determines the threshold ϵ through binary search, using depth of 20 evaluations of an exact acyclicity test to find the largest possible DAG for each method. NO-TEARS and NO-TEARS-LR's ϵ are chosen to be 0.3 while DCDI's is set to 0.5 as recommended by the respective authors. For DCDI, NO-TEARS and NO-TEARS-LR different thresholdings such as binary search are attempted without meaningful change to the result. Different fixed values for ϵ were also experimented for DCDFG without improvements. The author of Bicycle did not include disclose the appropriate threshold. We found the threshold of 0.005 to be the only one yielding reasonable results.

PerturbODE's ϵ threshold is determined using the formula $\epsilon = c \cdot \sigma$, where σ represents the standard deviation of the inferred GRN matrix \mathbf{G} across all entries, and c is a positive scalar. For SERGIO simulated data with 400 genes, $c = 1$, and for that with 100 genes, $c = 0.1$. For TF Atlas, we set $c = 0.1$.

As the authors of GENIE3 did not recommend a default threshold, we choose a threshold for GENIE3 in the same manner as PerturbODE. For SERGIO simulated data with 400 genes, $c = 5$, and for that with 100 genes, $c = 0.1$. Lastly, for TF Atlas, $c = 1$.

In simulated data, c is chosen so that the number of predicted edges approximately match the number of edges in the ground truth GRN. And for TF Atlas, c is chosen so that GENIE3 and PerturbODE predict a similar number of edges.

In SERGIO simulated data, we used ground truth networks that contain only positive edges. For the TF Atlas, the literature-curated GRN edges consist only of positive edges. PerturbODE and Bicycle can distinguish positive and negative edges, whereas DCDI and DCDFG only identify edge existence. When evaluating PerturbODE and Bicycle on SERGIO simulated data, we treat incorrect sign as a false positive.

BoolODE simulated data contains both positive and negative edges. Hence, we take the absolute values over reference GRN and predicted GRN before comparison.

A.6.2 Thresholded Performance

PerturbODE demonstrates significantly higher precision, recall, and F1 scores compared to DCDFG, NO-TEARS, and NO-TEARS-LR, while performing comparably to DCDI in these metrics (Fig. 10, Fig. 9). DCDI is the state-of-the-art method that outperforms PerturbODE in lower dimensional simulated datasets (100 – 400 genes), but it lacks scalability. In fact, for dimensions greater than 400, DCDI simply fails to execute, even with the more computationally feasible spectral radius acyclicity constraint. Details of the performance across all models with varying numbers of modules are provided in A.6.3. PerturbODE’s main contribution is its ability to train on real datasets with thousands of genes, while maintaining competitive predicative performance.

For evaluation, we threshold the weights of the output GRNs to obtain classification metrics (details in Appendix A.6.1). To further address the discrepancies between graph sparsity and predictive performance, we employed random graphs to generate an empirical null for each test statistic for random graphs with the same edge density. We compare the precision-recall test statistics of the predicted GRN against those from 10,000 Erdős-Rényi random networks, yielding empirical p -values (for details, see Appendix A.4).

There is considerable variation in recall scores for PerturbODE especially in the simulated yeast dataset. This is likely due to the high sparsity in the ground truth GRN, which leads to weak signals in the simulated dataset. This results in false negatives. Further, L_1 penalty is enforced on the individual matrix. As multiplication of sparse matrices is not always sparse, the number of predicted edges tend to fluctuate. Denser predictions would have higher recall scores.

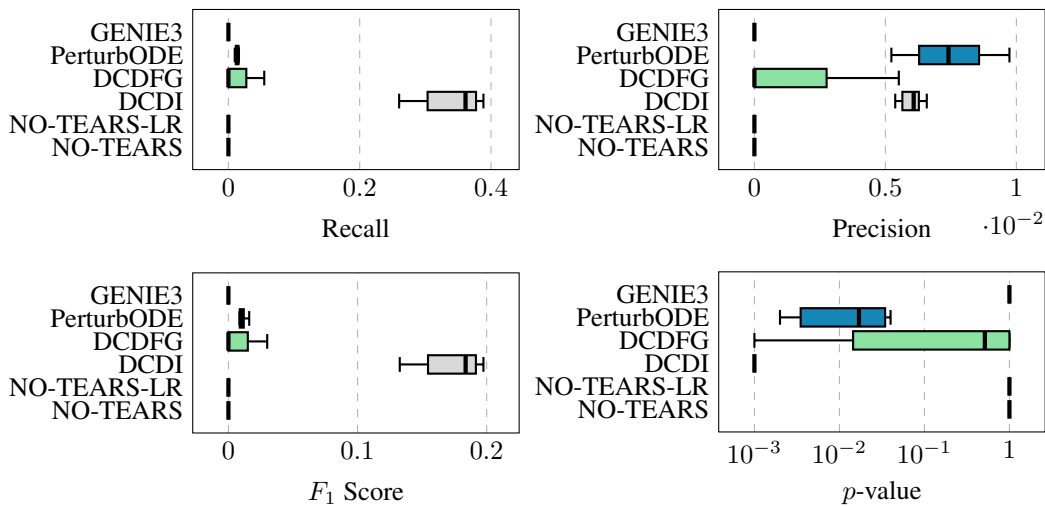


Figure 9: Performance metrics on SERGIO-simulated data of a known yeast GRN (400 genes), assuming perfect intervention over-expression (CRISPR-a).

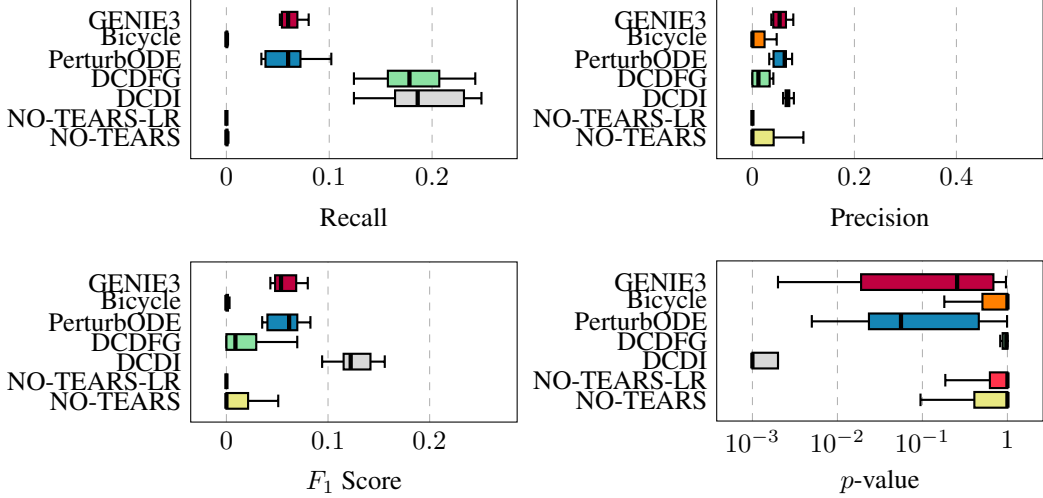


Figure 10: Performance metrics on SERGIO-simulated data of 10 random acyclic GRNs (100 genes), assuming perfect intervention over-expression (CRISPR-a).

Table 3: Average number of edges predicted by all methods across datasets

METHOD	GROUND TRUTH	PERTURBODE	NO-TEARS	NO-TEARS-LR	DCDI	DCDFG	GENIE3
YEAST GRN ($dim = 400$)	623	1205.8	0.0	0.0	24332.8	4293.8	721.6
RANDOM DAGS ($dim = 100$)	500	552.0	0.0	7.1	1423.7	215.1	586.2
TF ATLAS ($dim = 812$)	N/A	101404.2	438.0	76.0	N/A	72884.0	93430.0

Table 3 presents the number of edges predicted by each model across different datasets using the aforementioned thresholds.

A.6.3 GRN Inference Results with Different Number of Modules

PerturbODE and NO-TEARS-LR maintain consistent performance across different numbers of modules, while DCDFG achieves its best results with 10 modules. Figures 11 and 12 illustrate the performance of all models across varying number of modules in the SERGIO and TF Atlas datasets. Here, the threshold for PerturbODE is set at $c = 0.1$.

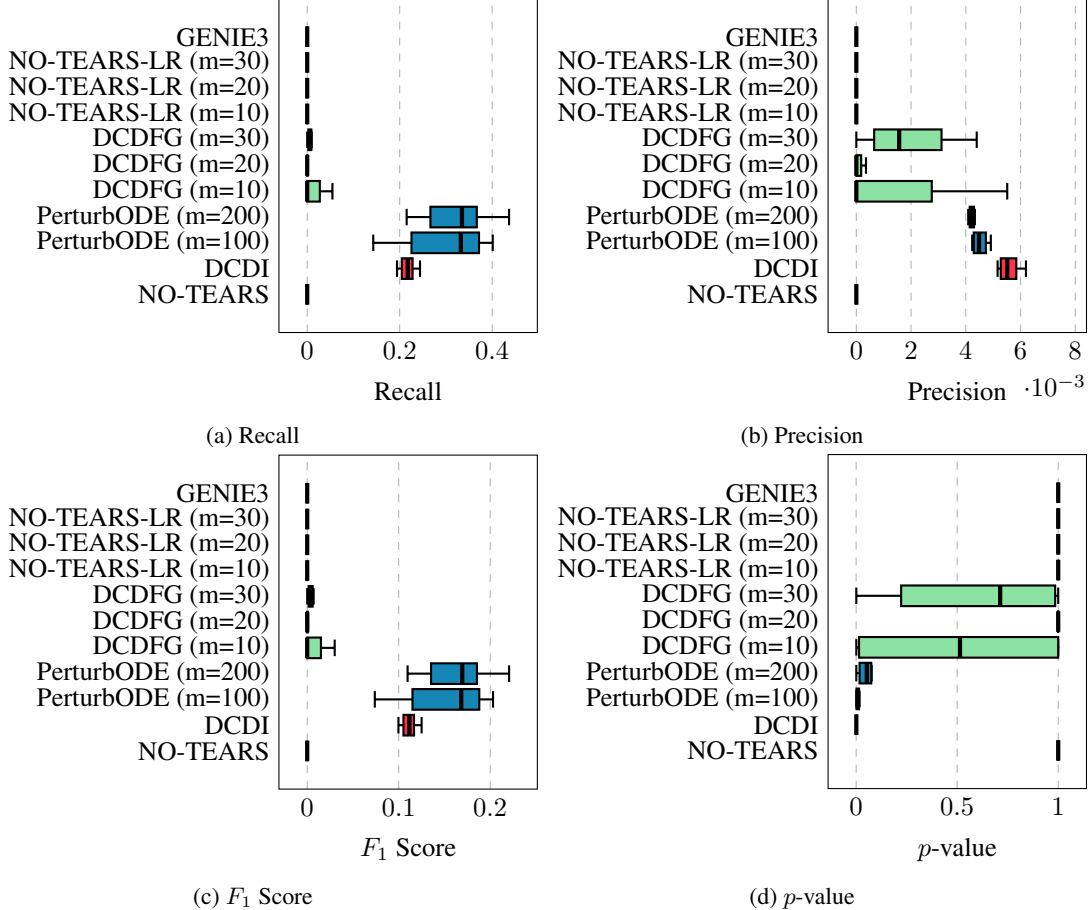


Figure 11: Perfect intervention over-expression (CRISPR-a) SERGIO simulation GRN inference. Ground truth GRN is a known yeast GRN (400 genes). Models with different number of modules are compared.

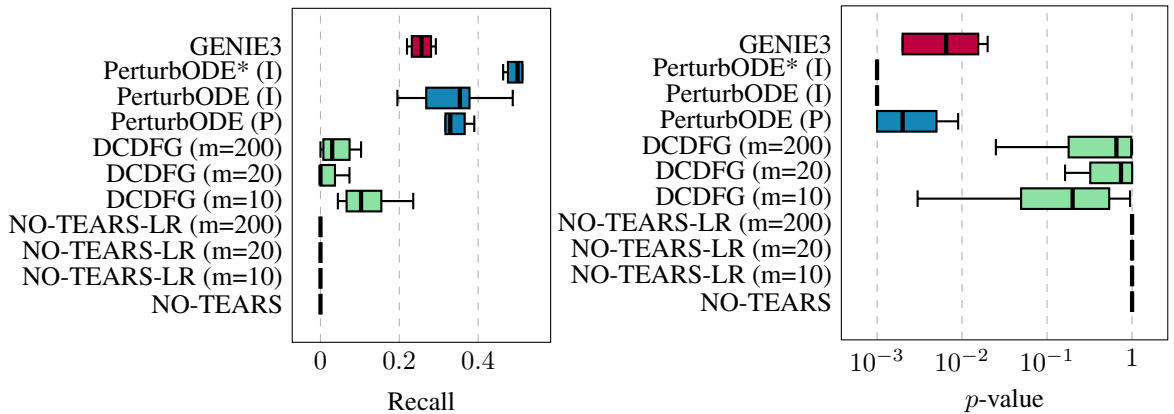


Figure 12: GRN Inference on TF Atlas Dataset (812 genes). Models with different numbers of modules are compared.

A.7 Additional Results

A.7.1 Mean and standard deviation of results

Table 4: Mean and standard deviation across models for yeast simulated by SERGIO

Method	Recall		Precision		AUPRC		F1		p-value	
	Mean	Std	Mean	Std	Mean	Std	Mean	Std	Mean	Std
GENIE3	0.0000	0.0000	0.0000	0.0000	0.0019	0.0000	0.0000	0.0000	1.0000	0.0000
PerturbODE	0.0151	0.0043	0.0079	0.0017	0.0045	0.0002	0.0115	0.0028	0.0458	0.0554
DCDFG	0.0315	0.0414	0.0026	0.0032	0.0041	0.0003	0.0170	0.0223	0.6058	0.4829
NO-TEARS-LR	0.0000	0.0000	0.0000	0.0000	0.0027	0.0015	0.0000	0.0000	1.0000	0.0000
NO-TEARS	0.0000	0.0000	0.0000	0.0000	0.0019	0.0000	0.0000	0.0000	1.0000	0.0000
DCDI	0.3499	0.0470	0.0061	0.0004	0.0059	0.0001	0.1780	0.0237	0.0010	0.0000

Table 5: Mean and standard deviation across models for random DAGs simulated by SERGIO

Method	Recall		Precision		AUPRC		F1		p-value	
	Mean	Std	Mean	Std	Mean	Std	Mean	Std	Mean	Std
GENIE3	0.0640	0.0098	0.0565	0.0143	0.0575	0.0058	0.0596	0.0117	0.4109	0.3712
DCDI	0.1960	0.0387	0.0695	0.0084	0.1528	0.0195	0.1327	0.0204	0.0145	0.0320
NO-TEARS-LR	0.0006	0.0013	0.0300	0.0605	0.0427	0.0190	0.0153	0.0308	0.8430	0.3144
DCDFG	0.0164	0.0188	0.0247	0.0251	0.0307	0.0203	0.0206	0.0214	0.8675	0.2923
PerturbODE	0.0622	0.0225	0.0579	0.0147	0.0521	0.0020	0.0601	0.0155	0.3039	0.3628
NO-TEARS	0.0006	0.0009	0.0683	0.1484	0.0530	0.0747	0.0345	0.0745	0.7911	0.3292

Table 6: Mean and standard deviation across models for TF Atlas

Method	Recall		p-value	
	Mean	Std	Mean	Std
GENIE3	0.2634	0.0284	0.0172	0.0182
NO-TEARS	0.0000	0.0000	1.0000	0.0000
NO-TEARS-LR	0.0000	0.0000	1.0000	0.0000
DCDFG	0.1353	0.0692	0.4158	0.3692
PerturbODE (imperfect interv)	0.3659	0.0556	0.0042	0.0032
PerturbODE* (imperfect interv)	0.4976	0.0195	0.0010	0.0000
PerturbODE (perfect interv)	0.3561	0.0946	0.0236	0.0452

A.8 Ablation Study & Power Analysis

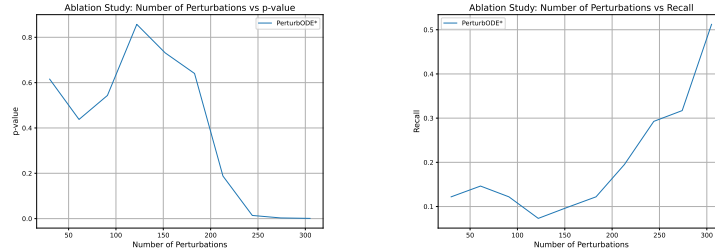


Figure 13: Ablation study: TF Atlas number of perturbations v.s. recall and p-value.

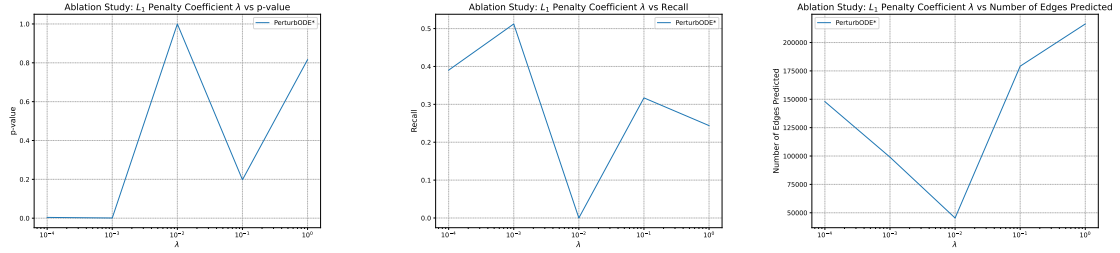


Figure 14: Ablation study: TF Atlas L_1 penalty coefficient λ v.s. recall, p-value, and number of edges predicted.

Ablation study is done for PerturbODE* trained on TF Atlas. Figure 13 shows the number of perturbations included for training plotted against recall and p-value. It is clear that as the number of perturbations grow, recall increases and p-value decreases. Figure 14 shows the change in recall and p-value when varying the L_1 penalty coefficient for B . Ablation study shows that PerturbODE* yields statistically significant result when $\lambda \leq 0.001$. Further, it is evident that as λ increases above 0.01, the number of edges predicted increase again. Our GRN is encoded as $\mathbf{G} = \mathbf{A} \text{diag}(\alpha) \mathbf{B}$. The multiplication of sparse matrices is not necessarily sparse. Further analysis shows strong penalization of B leads to overly dense A , as the model resorts to A for data fitting. This could lead to a rise of the number of edges predicted.

A.8.1 Prediction on Seen Intervention All UMAP and PCA Plots

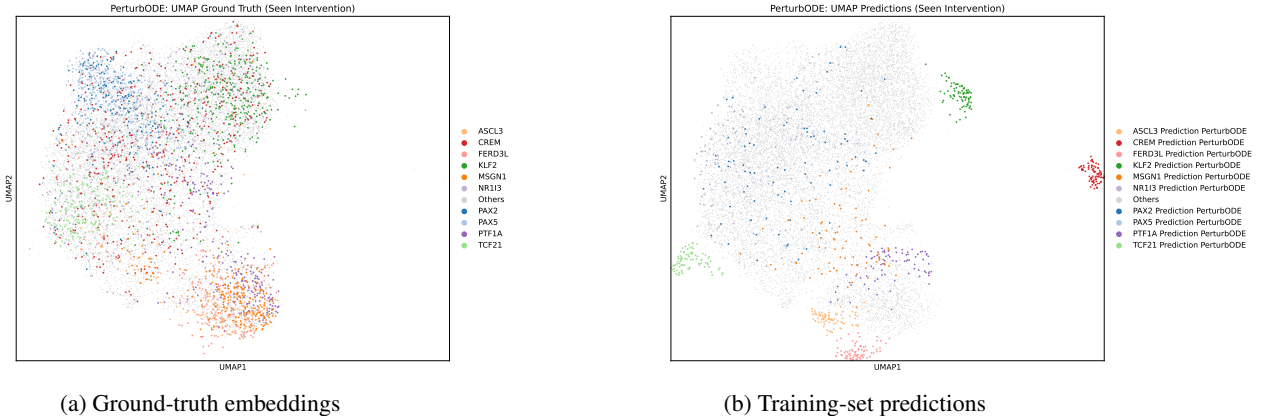


Figure 15: UMAP projections of cell embeddings: 10 transcription factors (TFs) from the training set, the model’s predictions on those TFs

A.8.2 Prediction on Unseen Intervention All UMAP and PCA Plots

Figures 16, 16, show the detailed results on prediction on test data (unseen intervention) through UMAP and PCA.

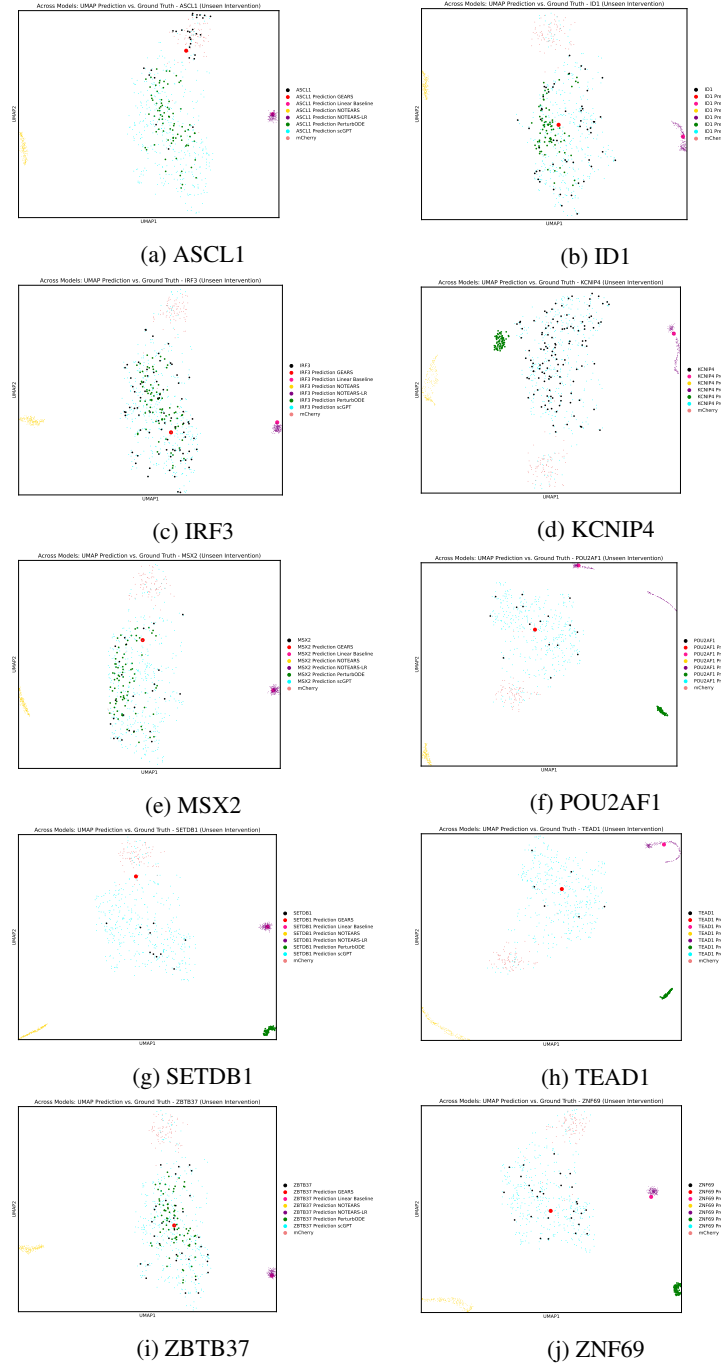


Figure 16: UMAP of predictions on unseen interventions across models.

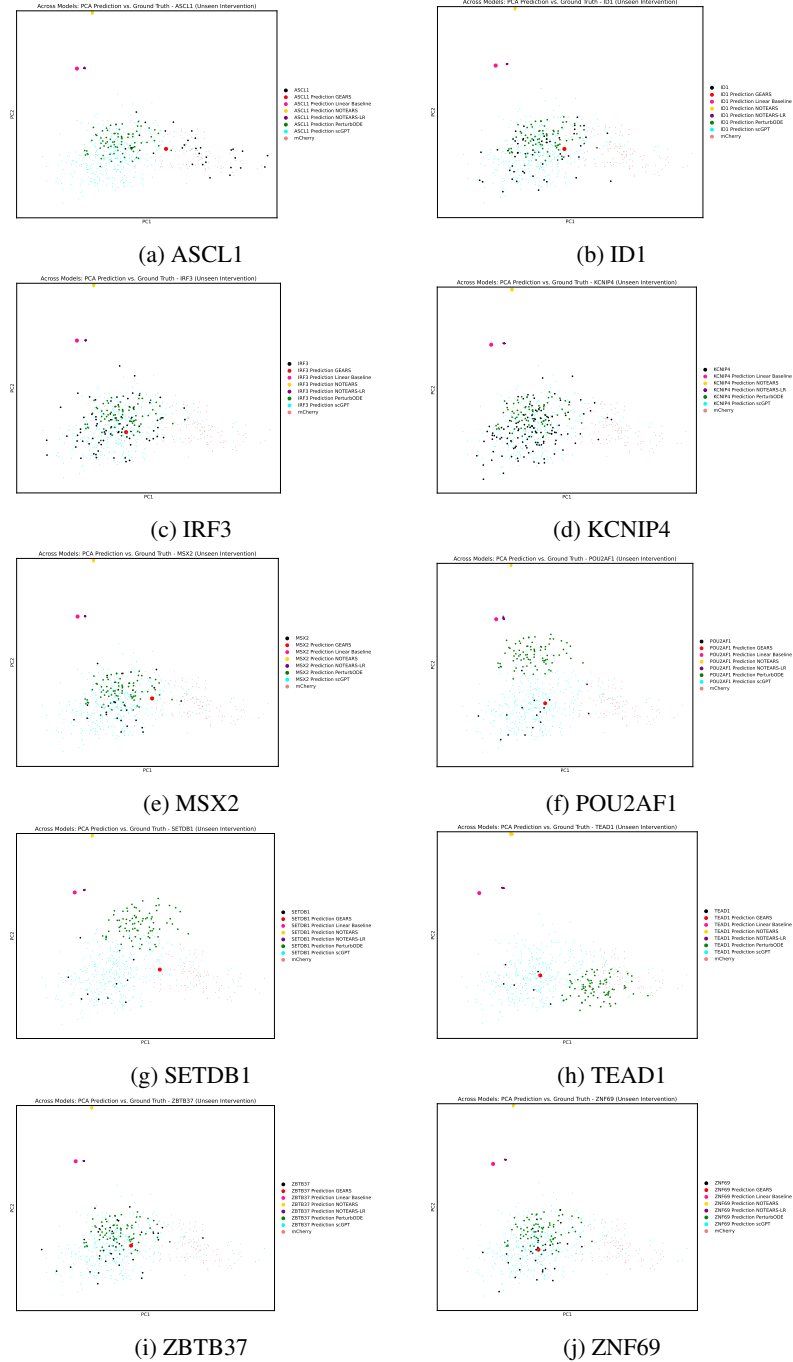


Figure 17: PCA of predictions on unseen interventions across models.

A.9 PerturbODE Model Training

After training, the average W_2 distance on both the training and held-out validation datasets decreases significantly and converges. The convergence rate of the W_2 distance varies for each TF in the training and validation sets.

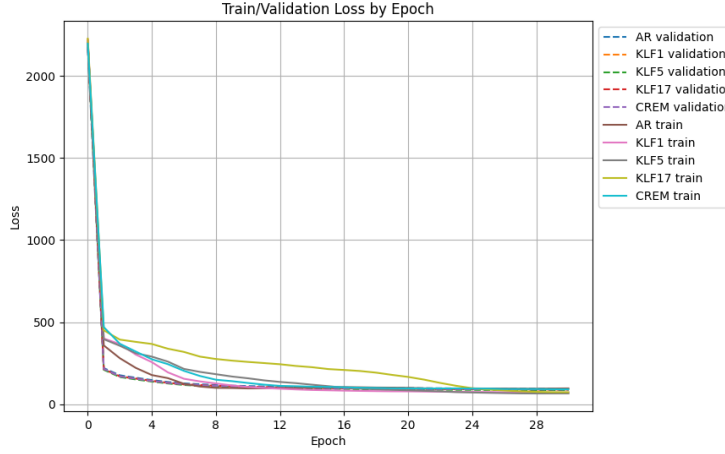


Figure 18: Convergence of W_2 losses for trajectory predictions of training and validation samples per TF. Average validation loss on TF Atlas is 78.88.

A.10 Ground truth GRNs from TF Atlas

The three GRNs with high confidence inferred in Joung et al. [2023] are consistent with their induced cell types and roles in development. GRHL1 and GRHL3 target TFAP2C and the TEAD family of TFs to induce trophoblasts, while FLI1 targets AP-1 family TFs (such as JUN and FOS) and ETV2 to induce vascular endothelial cells [Krendl et al., 2017, Dejana et al., 2007]. The GRN consisting of CDX1, CDX2, and HOXD11-influences posterior HOX genes is known to contribute to the definition of the anterior-posterior axis [Neijts et al., 2017]. The three GRNs are in Figures 19, 20, 21. These GRNs are further supported by ATAC-seq peaks and motif analysis, as confirmed by Joung et al. [2023].

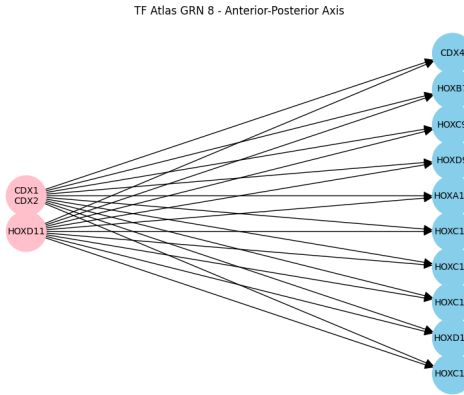


Figure 19: GRN with high confidence from TF Atlas - GRN8

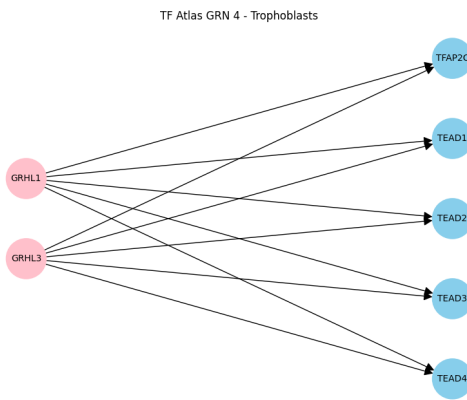


Figure 20: GRN with high confidence from TF Atlas - GRN4

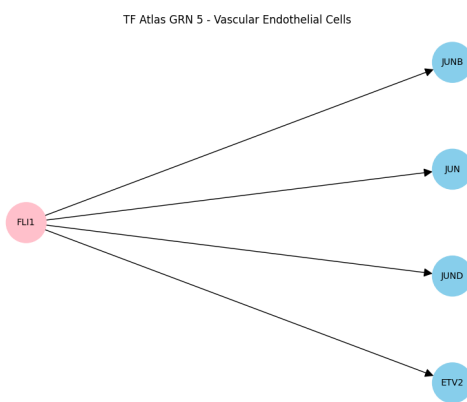


Figure 21: GRN with high confidence from TF Atlas - GRN5

A.11 Inferred Modules Encapsulating Ground Truth GRNs

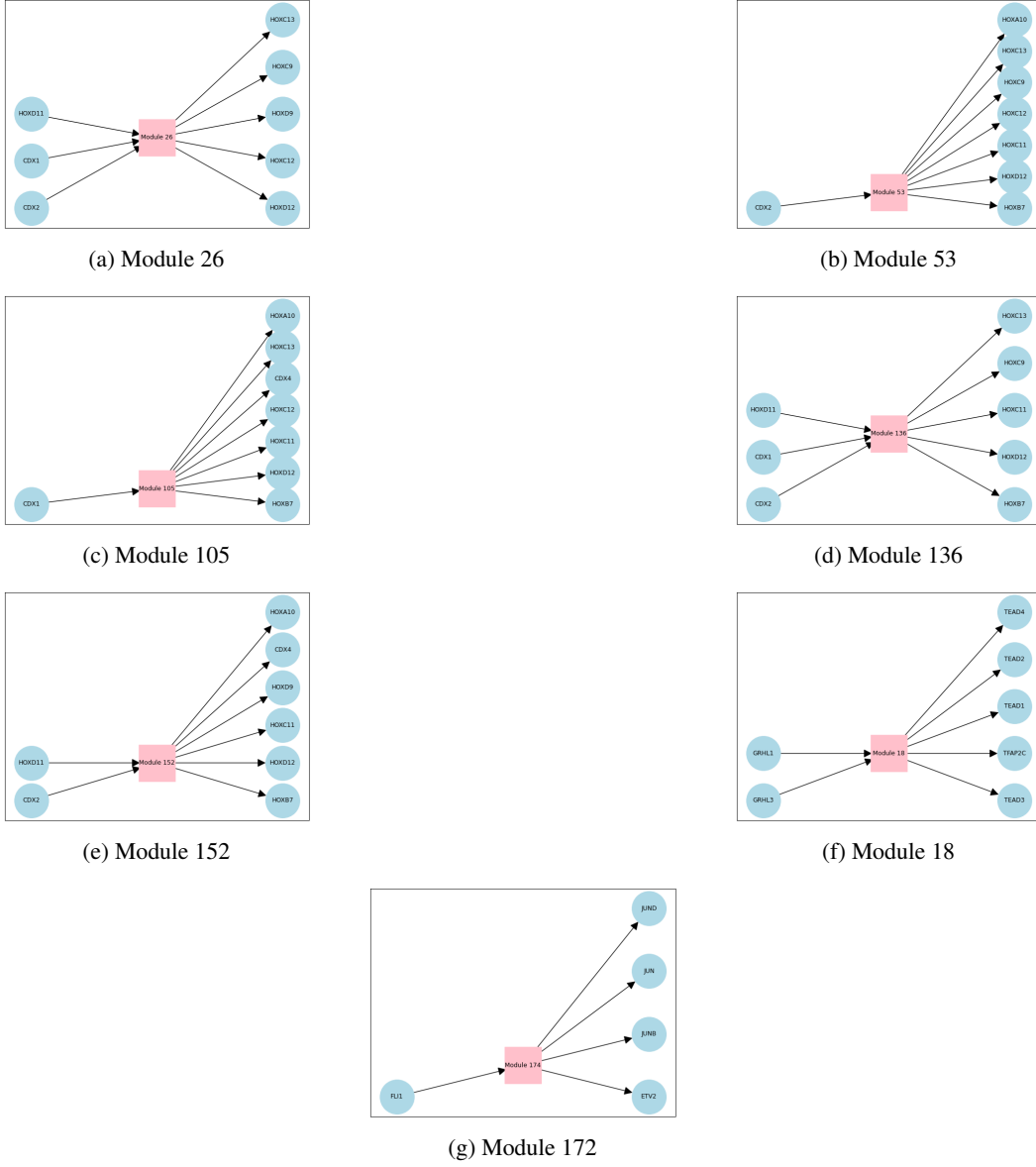


Figure 22: Modules identified by PerturbODE that align with established regulatory relationships.

A.11.1 Analysis of inferred gene modules

PerturbODE’s framework enables direct interpretation of the inferred gene modules, which encapsulate multiple gene to gene interactions. These interactions are extracted from the A and B matrices (Equation 1), where the entries in B represent directed edges from upstream genes to gene modules, and the entries in A map the modules to downstream genes.

To highlight the advantages of PerturbODE’s interpretability, we analyze the 200 inferred latent gene modules obtained from training on the TF Atlas dataset. We computed a test score based on the number of correct gene regulators and targets in the GRN selected by each module (Section A.4). We visualize seven modules with the highest scores in Figure 22, each corresponding to directed edges found in experimentally validated GRNs (Appendix A.10). The modules in (a) - (e) encapsulate the GRN responsible for specification of the anterior-posterior axis in development [Neijts et al., 2017]. (f) and (g) successfully capture known GRNs responsible for inducing trophoblasts and vascular

endothelial cells respectively [Krendl et al., 2017, Dejana et al., 2007]. Additionally, we compared the inferred modules to Erdős-Rényi random matrices in terms of the number of correct regulators and targets selected, yielding p -values of less than 0.001 (Appendix A.4). Significant p -values indicate that the correct genes are not assigned to the modules by random chance. By inspecting the modules, we demonstrate that PerturbODE recovers the appropriate gene network structure, clustering genes from the same GRN and accurately inferring edges between them.

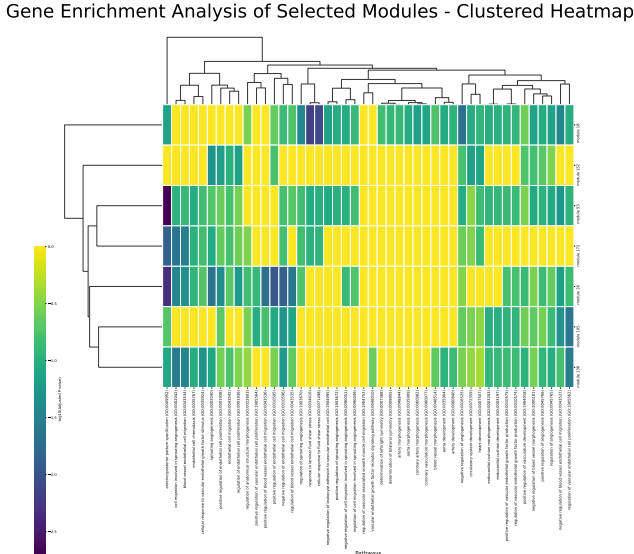


Figure 23: Gene enrichment clustered heatmap (average linkage) for selected modules.

We further validate PerturbODE’s inferred gene modules through gene set enrichment analysis (GSEA), which evaluates the overlap between genes associated with known biological pathways and genes within each predicted module. Figure 23 presents a clustered heatmap of statistically significant pathway enrichments across modules (a) to (g), with details provided in Appendix A.11.2. Our analysis reveals biologically coherent patterns that align with cellular differentiation. Modules 172 and 136 show enrichment in pathways specific to vascular endothelial cells. Meanwhile, modules 26, 172, 136, 18, and 53 demonstrate strong enrichment in anterior-posterior (A-P) axis specification, with module 53 showing the strongest significance. Additionally, module 18 exhibits significant enrichment in pathways related to angiogenesis and fluid stress response.

A.11.2 Full Gene Enrichment Analysis

We performed gene enrichment analysis using the Reactome Pathway Database (2022) and the Gene Ontology Biological Process (2021) with hypergeometric test. The examined pathways were filtered to those relevant to the anterior-posterior axis and vascular endothelial cells. The upstream genes and downstream genes of each module are selected by taking those edges whose weights are greater than 2 standard deviations of B and A respectively. Figure 26 illustrates the clustering of modules based on specific functions. A significant number of modules exhibit enrichment for anterior-posterior specification—a pathway crucial in development. This observation is expected, considering that the TF Atlas comprises human embryonic stem cells.

To show that the modules are not selecting identical genes, we plotted histograms of genes selected by various modules. Figure 24 shows a histogram of genes selected by the highlighted modules we selected for evaluation in Section A.11.1, and Figure 25 showcases that of 10 randomly selected modules. Both histograms show clear clustering of gene selections by modules.

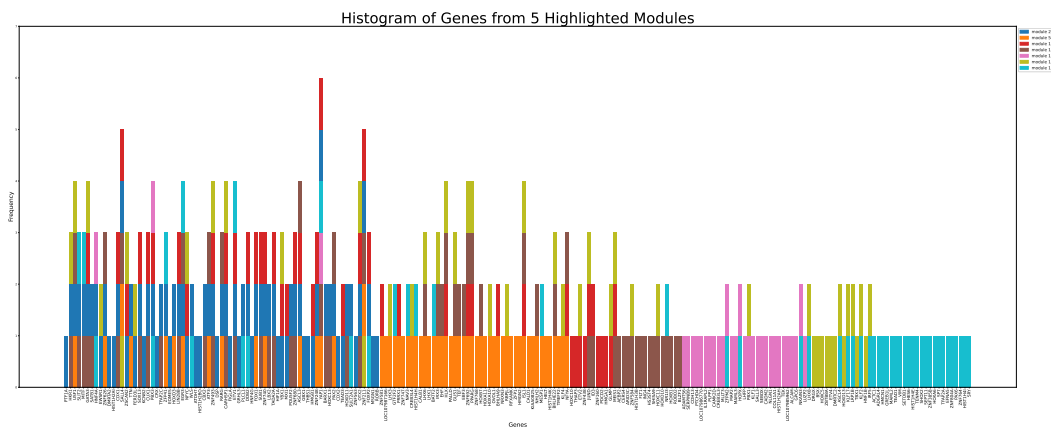


Figure 24: Histogram of Genes from 5 Highlighted Modules.

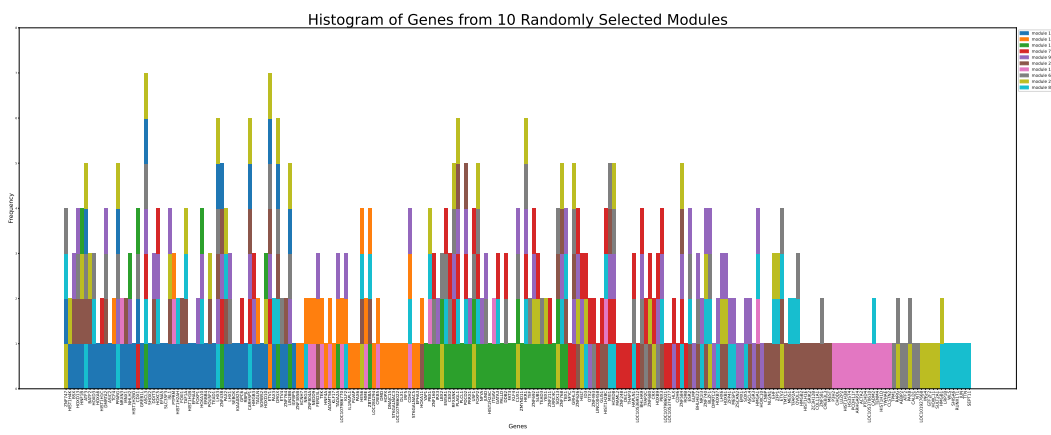


Figure 25: Histogram of Genes from 10 Randomly Selected Modules.

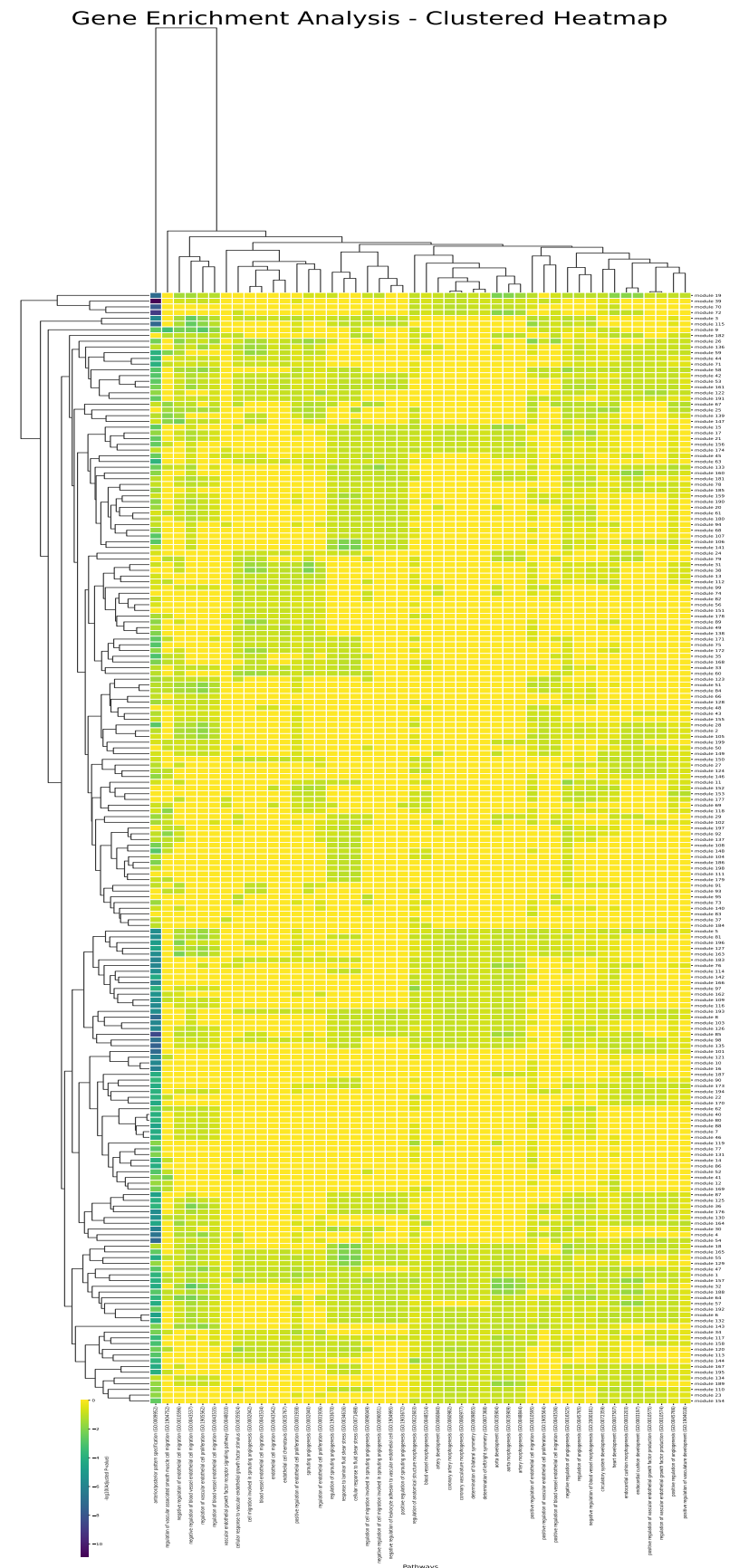


Figure 26: Gene enrichment clustered heatmap (average linkage) for all modules.

A.12 SERGIO simulation

SERGIO proposes simulation of scRNA-seq data by sampling a directed acyclic GRN through a SDE [Dibaeinia and Sinha, 2020]. Although SERGIO does not support interventional data, we modified its framework to simulate gene over-expression with perfect interventions (CRISPR-a). For each interventional regime $I \in \mathcal{I}$, the SDE is parameterized in the following Equation 8.

$$dX_t = \left(M \left(P(X_t) - \lambda \circ X_t \right) + \sum_{j \in I} \gamma_j \cdot \delta_j \right) dt + q \circ \left(\sqrt{P(X_t)} dW_\alpha + \sqrt{\lambda X_t} dW_\beta \right) \quad (8)$$

The infinitesimal change of expression level (which is the stochastic process X_t) of gene j at time t over an infinitesimal time interval dt , denoted as $(dX_t)_j$, is governed by its production rate $P_j(X_t)$, which is modulated by its regulators according to a given GRN in Equation 9. It also depends on the decay rate $\lambda \in \mathbb{R}_+^d$ and the noise amplitude $q \in \mathbb{R}^d$ influencing its transcriptional variability. M and $\sum_{j \in I} \gamma_j \cdot \delta_j$ are the masking matrix and the over-expression term analogous to those in Equations 1 and 2.

$$P_j(X) = \sum_{i=0}^d p_{ji}(X) + b_j \quad \text{for } p_{ji} \text{ in 10, 11} \quad (9)$$

$$p_{ji}(X) = K_{ji} \frac{X_i}{h + X_i} \quad \text{if regulator } i \text{ is an activator of gene } j \quad (10)$$

$$p_{ji}(X) = K_{ji} \left(1 - \frac{X_i}{h + X_i} \right) \quad \text{if regulator } i \text{ is a repressor of gene } j \quad (11)$$

For each pair of genes i and j , the coefficients are initialized as in 12.

$$\begin{aligned} \lambda_j &\sim \mathcal{N}(0.8, 0.2)_+ \quad , \quad K_{ji} \sim \mathcal{U}(0, 5) \quad , \quad q_j \sim \mathcal{U}(0.3, 1) \quad , \quad \gamma_j \sim \mathcal{N}(10, 1)_+ \quad , \\ h &= \frac{1}{d} \sum_{j=0}^d \frac{b_j}{q_j} \quad , \\ b_j &\sim \mathcal{N}(10, 0.01)_+ \quad \text{if gene } j \text{ is a master regulator,} \\ b_j &= 0 \quad \text{if gene } j \text{ is not a master regulator.} \end{aligned} \quad (12)$$

$W_\alpha, W_\beta \in \mathbb{R}^d$ are two independent Wiener processes. We numerically simulate the SDE in Equation 8 using the Euler-Maruyama Scheme [E et al., 2019] with $\Delta t = 2$ in 50 steps.

$$\begin{aligned} (X_j)_{t+\Delta t} &= (X_j)_t + \left(\left(P_j(X_t) - \lambda_j X_j(t) \right) \cdot \mathbb{I}_{j \notin I} + \gamma_j \cdot \mathbb{I}_{j \in I} \right) \Delta t \\ &\quad + q_j \sqrt{P_j(X_t)} \Delta W_\alpha + q_j \sqrt{\lambda_j X_j(t)} \Delta W_\beta \end{aligned} \quad (13)$$

$$(\Delta W_\alpha)_j \sim \sqrt{\Delta t} \mathcal{N}(0, 1), \quad (\Delta W_\beta)_j \sim \sqrt{\Delta t} \mathcal{N}(0, 1) \quad (14)$$

Lastly, the SDE 8 is initialized at the expected fixed point X_0 (where the drift of the SDE vanishes) with over-expression but without masking (perfect intervention). SERGIO assumes Jansen's Equality $E[p_{ji}(X_i)] \approx p_{ji}(E[X_i])$ for simplicity of initialization [Dibaeinia and Sinha, 2020]. Hence, X_0 is initialized to the following expectations in Equations 15 and 16:

$$E[X_j] = \frac{\sum_{i=0}^d p_{ji}(E[X_i])}{\lambda_j} + \gamma_j \cdot \mathbb{I}_{j \in I} \quad \text{if } j \text{ is not a master regulator} \quad (15)$$

$$E[X_j] = \frac{b_i}{\lambda_j} + \gamma_j \cdot \mathbb{I}_{j \in I} \quad \text{if gene } j \text{ is a master regulator} \quad (16)$$

When simulating data using SERGIO, we use a real yeast GRN ($dim = 400$) and 10 random DAGs ($dim = 100$) with 500 binary entries (1 or 0). For clarity of comparison across models, the real yeast GRN is pruned to enforce acyclicity and include only positive directed edges. For both scenarios, the synthetic dataset generated by SERGIO includes 10,100 cells, created from 100 intervention schemes, each targeting 5 genes, along with one non-intervention scheme. Each regime provides 100 observations.

A.13 BoolODE simulation

BoolODE [Pratapa et al., 2020] is a single-cell RNA-seq simulator that models mRNA dynamics using stochastic differential equations (SDEs), where gene regulatory interactions are represented through Hill functions approximating Boolean logic. Here, x_i denotes the mRNA concentration of gene i , p_i represents its corresponding protein level, and R_i reflects the concentration of regulatory proteins controlling gene i . The coefficients m , r , l_p , l_x , and s are constants, while $f(\cdot)$ captures the regulatory relationships within the GRN. The SDE system is defined as:

$$\frac{d[x_i]}{dt} = mf(R_i) - l_x[x_i] + s\sqrt{[x_i]}dB_t \quad (17)$$

$$\frac{d[p_i]}{dt} = r[x_i] - l_p[p_i] + s\sqrt{[p_i]}dB_t \quad (18)$$

Following the approach in SERGIO, we simulate perturbations by performing perfect interventions combined with overexpression (CHRIPR-a). This involves suppressing the regulatory influence of the target gene in $f(\cdot)$ while introducing an additive shift to model overexpression. The over-expression is set to 20. This generates a collection of distributions in gene expression space, with each distribution corresponding to a distinct interventional condition. The environments include an observational (no-intervention) setting and multiple interventional settings where each gene is individually targeted. The resulting empirical distributions are denoted as $\{\rho_i\}_{i=0}^k$. The coefficients are set to the default given by the authors, where $r = 10$, $s = 10$, $l_x = 10$, $l_p = 10$, and $m = 20$.

We utilized the toy-GRN with bifurcating convergent behavior manually curated by the authors. We simulated 300 cells for each perturbation, and the simulation time is set to 1000 to encourage steady-state distributions of cells. There are 10 genes in this prescribed system, and we simulated perturbations with a single gene at a time for all 10 genes. We also simulated an observational distribution without perturbations.

A.14 Gene Module Example: Flagella of E. coli

It is well established that the regulatory circuit responsible for the production of E. coli follows the network motif of multiple-output Feedforward Loop [Alon, 2006, pp. 64-68]. Its circuit is shown on the left of Figure 27, where FlhDC and FliA regulate Z_1 , Z_2 , and Z_3 , which are operons encoding the proteins that make up the flagella of E. coli. (In fact, there are in total 6 operons for this process.) Each operon consists of a group of genes, and it is regulated by a weighted sum of non-linearly activated signals from FlhDC and FliA through Hill functions.

The order in which the operons are activated matches the order of proteins needed to assemble the flagella. The timing of activation is achieved by different activation thresholds in the Hill functions. If Z_1 is activated before Z_2 , which is activated before Z_3 , then $K_2 < K_3 < K_4$. In other words, Z_1 needs a lower concentration of FliA to be switched on. For example, Z_1 would include the group of genes encoding the proteins for MS ring (base of flagella) and Z_3 would be for the filament (tail of flagella). In PerturbODE, the activation threshold is tuned by the bias term, β , to the hidden neurons.

This structure can be represented in a two-layer MLP shown on the right of Figure 27. Each operon Z_i is regulated by the weighted sum of signals from two modules M_i and M'_i . The signals from FliA and FlhDC are first activated by Hill functions with different activation thresholds before being transferred to modules M_i and M'_i respectively.

To represent this gene regulatory circuit with an adjacency matrix $\mathbf{G} = A \text{ diag}(\alpha)B$, we multiply the two coefficient weight matrices of the MLP with an additional scaling to account for the rate of activation controlled by α .

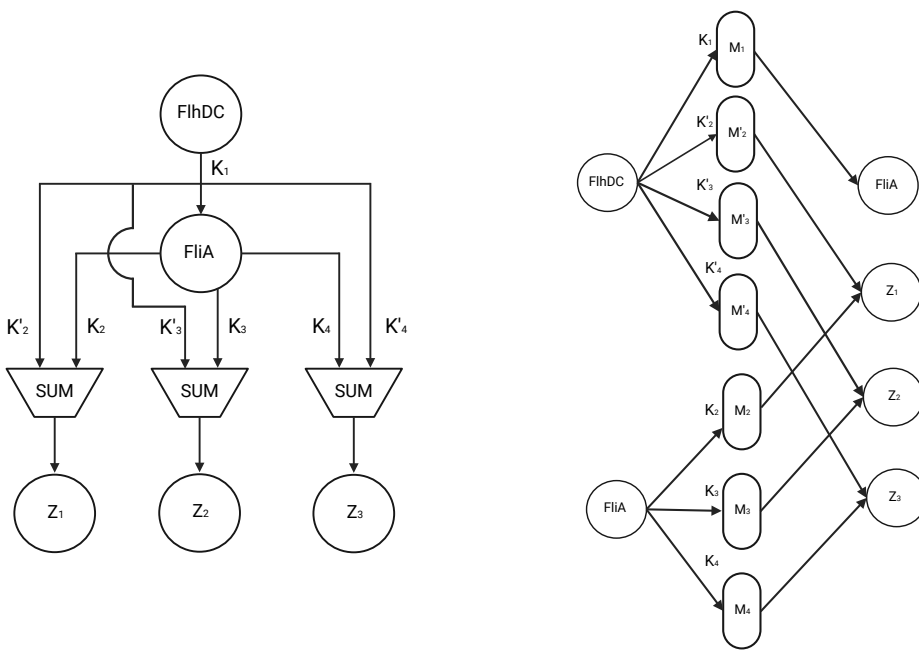


Figure 27: Regulatory circuit for the production of flagella in *E. coli*.

A.15 Statistical Inference: Generalizability and Stability Analysis

For stability analysis, we bootstrapped (sampled with replacement) TF Atlas dataset 105 times to evaluate consistency in the edges selected by PerturbODE. We also filtered the list of TFs perturbations that PerturbODE trains on down to the TFs pertinent to the ground truth GRNs in order to reduce training time. Then the gene expression space is the union between the filtered TF list and the top 50 highly variable genes, resulting in 52 genes. For generalizability analysis, we performed a similar procedure but using 133 different train-validation split. Train-validation split is chosen to be 8-2, where, for each interventional distribution, 20% of samples are withheld for the validation set. The validation set is used as stopping criterion (a hyper-parameter) for training.

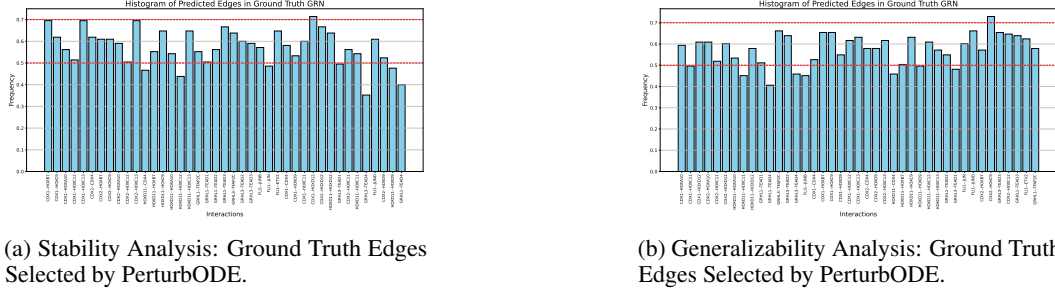


Figure 28: Comparison of Stability and Generalizability Analyses for Ground Truth Edges Selected by PerturbODE.

Figures 28a and 28b indicate that PerturbODE selects the ground truth edges roughly 50% to 70% of the time in both the stability and generalizability analyses. While a highly consistent model would ideally surpass a 75% selection rate, these results nonetheless reflect a reasonable degree of reliability given the inherent complexity of the task. Future enhancements to the model may further improve this consistency.

A.16 Cell-Type Distance

We provide a new metric to assess the accuracy of cell-type prediction. We first average the gene expression values across all cells and classify the cell type of the averaged expression using k-nearest neighbor search ($k = 10$) in a 50-dimensional PCA space. The classification result produces a categorical vector c representing the probabilities of each cell type. Our cell-type distance is then defined as the L_1 distance $\|\hat{c} - c\|_1$, where \hat{c} is the classification vector for our predicted distribution and c is the vector for the observed distribution. A smaller distance indicates a better alignment of the cell type between our predictions and ground truth.

A.17 Compute Resource

All methods except GENIE3 were run on GPU nodes with V100 GPU cards (32 GB memory), with a maximum runtime of 24 hours per experiment. GENIE3 was executed on a CPU with 50 GB of memory and a runtime limit of 72 hours. Storage needed for the TF Atlas dataset is 4.1 GB.

NeurIPS Paper Checklist

1. Claims

Question: Do the main claims made in the abstract and introduction accurately reflect the paper's contributions and scope?

Answer: [\[Yes\]](#)

Justification: This paper proposes a novel framework to capture causal interactions from large scale perturbational data by modeling cell state trajectories.

Guidelines:

- The answer NA means that the abstract and introduction do not include the claims made in the paper.
- The abstract and/or introduction should clearly state the claims made, including the contributions made in the paper and important assumptions and limitations. A No or NA answer to this question will not be perceived well by the reviewers.
- The claims made should match theoretical and experimental results, and reflect how much the results can be expected to generalize to other settings.
- It is fine to include aspirational goals as motivation as long as it is clear that these goals are not attained by the paper.

2. Limitations

Question: Does the paper discuss the limitations of the work performed by the authors?

Answer: [\[Yes\]](#)

Justification: This work discusses future improvements, such as the incorporation biological priors which can include functional gene annotations. We also demonstrate lower-dimensional settings in which the model does not perform the best.

Guidelines:

- The answer NA means that the paper has no limitation while the answer No means that the paper has limitations, but those are not discussed in the paper.
- The authors are encouraged to create a separate "Limitations" section in their paper.
- The paper should point out any strong assumptions and how robust the results are to violations of these assumptions (e.g., independence assumptions, noiseless settings, model well-specification, asymptotic approximations only holding locally). The authors should reflect on how these assumptions might be violated in practice and what the implications would be.
- The authors should reflect on the scope of the claims made, e.g., if the approach was only tested on a few datasets or with a few runs. In general, empirical results often depend on implicit assumptions, which should be articulated.
- The authors should reflect on the factors that influence the performance of the approach. For example, a facial recognition algorithm may perform poorly when image resolution is low or images are taken in low lighting. Or a speech-to-text system might not be used reliably to provide closed captions for online lectures because it fails to handle technical jargon.
- The authors should discuss the computational efficiency of the proposed algorithms and how they scale with dataset size.
- If applicable, the authors should discuss possible limitations of their approach to address problems of privacy and fairness.
- While the authors might fear that complete honesty about limitations might be used by reviewers as grounds for rejection, a worse outcome might be that reviewers discover limitations that aren't acknowledged in the paper. The authors should use their best judgment and recognize that individual actions in favor of transparency play an important role in developing norms that preserve the integrity of the community. Reviewers will be specifically instructed to not penalize honesty concerning limitations.

3. Theory assumptions and proofs

Question: For each theoretical result, does the paper provide the full set of assumptions and a complete (and correct) proof?

Answer: [NA]

Justification: This paper does not include theoretical contribution.

Guidelines:

- The answer NA means that the paper does not include theoretical results.
- All the theorems, formulas, and proofs in the paper should be numbered and cross-referenced.
- All assumptions should be clearly stated or referenced in the statement of any theorems.
- The proofs can either appear in the main paper or the supplemental material, but if they appear in the supplemental material, the authors are encouraged to provide a short proof sketch to provide intuition.
- Inversely, any informal proof provided in the core of the paper should be complemented by formal proofs provided in appendix or supplemental material.
- Theorems and Lemmas that the proof relies upon should be properly referenced.

4. Experimental result reproducibility

Question: Does the paper fully disclose all the information needed to reproduce the main experimental results of the paper to the extent that it affects the main claims and/or conclusions of the paper (regardless of whether the code and data are provided or not)?

Answer: [Yes]

Justification: See Appendix A.3.

Guidelines:

- The answer NA means that the paper does not include experiments.
- If the paper includes experiments, a No answer to this question will not be perceived well by the reviewers: Making the paper reproducible is important, regardless of whether the code and data are provided or not.
- If the contribution is a dataset and/or model, the authors should describe the steps taken to make their results reproducible or verifiable.
- Depending on the contribution, reproducibility can be accomplished in various ways. For example, if the contribution is a novel architecture, describing the architecture fully might suffice, or if the contribution is a specific model and empirical evaluation, it may be necessary to either make it possible for others to replicate the model with the same dataset, or provide access to the model. In general, releasing code and data is often one good way to accomplish this, but reproducibility can also be provided via detailed instructions for how to replicate the results, access to a hosted model (e.g., in the case of a large language model), releasing of a model checkpoint, or other means that are appropriate to the research performed.
- While NeurIPS does not require releasing code, the conference does require all submissions to provide some reasonable avenue for reproducibility, which may depend on the nature of the contribution. For example
 - (a) If the contribution is primarily a new algorithm, the paper should make it clear how to reproduce that algorithm.
 - (b) If the contribution is primarily a new model architecture, the paper should describe the architecture clearly and fully.
 - (c) If the contribution is a new model (e.g., a large language model), then there should either be a way to access this model for reproducing the results or a way to reproduce the model (e.g., with an open-source dataset or instructions for how to construct the dataset).
 - (d) We recognize that reproducibility may be tricky in some cases, in which case authors are welcome to describe the particular way they provide for reproducibility. In the case of closed-source models, it may be that access to the model is limited in some way (e.g., to registered users), but it should be possible for other researchers to have some path to reproducing or verifying the results.

5. Open access to data and code

Question: Does the paper provide open access to the data and code, with sufficient instructions to faithfully reproduce the main experimental results, as described in supplemental material?

Answer: [No]

Justification: Code with instructions on reproducing results will be released.

Guidelines:

- The answer NA means that paper does not include experiments requiring code.
- Please see the NeurIPS code and data submission guidelines (<https://nips.cc/public/guides/CodeSubmissionPolicy>) for more details.
- While we encourage the release of code and data, we understand that this might not be possible, so “No” is an acceptable answer. Papers cannot be rejected simply for not including code, unless this is central to the contribution (e.g., for a new open-source benchmark).
- The instructions should contain the exact command and environment needed to run to reproduce the results. See the NeurIPS code and data submission guidelines (<https://nips.cc/public/guides/CodeSubmissionPolicy>) for more details.
- The authors should provide instructions on data access and preparation, including how to access the raw data, preprocessed data, intermediate data, and generated data, etc.
- The authors should provide scripts to reproduce all experimental results for the new proposed method and baselines. If only a subset of experiments are reproducible, they should state which ones are omitted from the script and why.
- At submission time, to preserve anonymity, the authors should release anonymized versions (if applicable).
- Providing as much information as possible in supplemental material (appended to the paper) is recommended, but including URLs to data and code is permitted.

6. Experimental setting/details

Question: Does the paper specify all the training and test details (e.g., data splits, hyper-parameters, how they were chosen, type of optimizer, etc.) necessary to understand the results?

Answer: [Yes]

Justification: See Appendix A.2 and A.3.

Guidelines:

- The answer NA means that the paper does not include experiments.
- The experimental setting should be presented in the core of the paper to a level of detail that is necessary to appreciate the results and make sense of them.
- The full details can be provided either with the code, in appendix, or as supplemental material.

7. Experiment statistical significance

Question: Does the paper report error bars suitably and correctly defined or other appropriate information about the statistical significance of the experiments?

Answer: [Yes]

Justification: Error bars are present in performance comparisons. We also use a statistical significance test for GRN predictions (see Appendix A.4).

Guidelines:

- The answer NA means that the paper does not include experiments.
- The authors should answer “Yes” if the results are accompanied by error bars, confidence intervals, or statistical significance tests, at least for the experiments that support the main claims of the paper.
- The factors of variability that the error bars are capturing should be clearly stated (for example, train/test split, initialization, random drawing of some parameter, or overall run with given experimental conditions).

- The method for calculating the error bars should be explained (closed form formula, call to a library function, bootstrap, etc.)
- The assumptions made should be given (e.g., Normally distributed errors).
- It should be clear whether the error bar is the standard deviation or the standard error of the mean.
- It is OK to report 1-sigma error bars, but one should state it. The authors should preferably report a 2-sigma error bar than state that they have a 96% CI, if the hypothesis of Normality of errors is not verified.
- For asymmetric distributions, the authors should be careful not to show in tables or figures symmetric error bars that would yield results that are out of range (e.g. negative error rates).
- If error bars are reported in tables or plots, The authors should explain in the text how they were calculated and reference the corresponding figures or tables in the text.

8. Experiments compute resources

Question: For each experiment, does the paper provide sufficient information on the computer resources (type of compute workers, memory, time of execution) needed to reproduce the experiments?

Answer: [\[Yes\]](#)

Justification: See Appendix A.17.

Guidelines:

- The answer NA means that the paper does not include experiments.
- The paper should indicate the type of compute workers CPU or GPU, internal cluster, or cloud provider, including relevant memory and storage.
- The paper should provide the amount of compute required for each of the individual experimental runs as well as estimate the total compute.
- The paper should disclose whether the full research project required more compute than the experiments reported in the paper (e.g., preliminary or failed experiments that didn't make it into the paper).

9. Code of ethics

Question: Does the research conducted in the paper conform, in every respect, with the NeurIPS Code of Ethics <https://neurips.cc/public/EthicsGuidelines>?

Answer: [\[Yes\]](#)

Justification: We follow the NeurIPS Code of Ethics.

Guidelines:

- The answer NA means that the authors have not reviewed the NeurIPS Code of Ethics.
- If the authors answer No, they should explain the special circumstances that require a deviation from the Code of Ethics.
- The authors should make sure to preserve anonymity (e.g., if there is a special consideration due to laws or regulations in their jurisdiction).

10. Broader impacts

Question: Does the paper discuss both potential positive societal impacts and negative societal impacts of the work performed?

Answer: [\[Yes\]](#)

Justification: See Appendix A.1

Guidelines:

- The answer NA means that there is no societal impact of the work performed.
- If the authors answer NA or No, they should explain why their work has no societal impact or why the paper does not address societal impact.
- Examples of negative societal impacts include potential malicious or unintended uses (e.g., disinformation, generating fake profiles, surveillance), fairness considerations (e.g., deployment of technologies that could make decisions that unfairly impact specific groups), privacy considerations, and security considerations.

- The conference expects that many papers will be foundational research and not tied to particular applications, let alone deployments. However, if there is a direct path to any negative applications, the authors should point it out. For example, it is legitimate to point out that an improvement in the quality of generative models could be used to generate deepfakes for disinformation. On the other hand, it is not needed to point out that a generic algorithm for optimizing neural networks could enable people to train models that generate Deepfakes faster.
- The authors should consider possible harms that could arise when the technology is being used as intended and functioning correctly, harms that could arise when the technology is being used as intended but gives incorrect results, and harms following from (intentional or unintentional) misuse of the technology.
- If there are negative societal impacts, the authors could also discuss possible mitigation strategies (e.g., gated release of models, providing defenses in addition to attacks, mechanisms for monitoring misuse, mechanisms to monitor how a system learns from feedback over time, improving the efficiency and accessibility of ML).

11. Safeguards

Question: Does the paper describe safeguards that have been put in place for responsible release of data or models that have a high risk for misuse (e.g., pretrained language models, image generators, or scraped datasets)?

Answer: [NA]

Justification: This paper poses no such risks for misuse.

Guidelines:

- The answer NA means that the paper poses no such risks.
- Released models that have a high risk for misuse or dual-use should be released with necessary safeguards to allow for controlled use of the model, for example by requiring that users adhere to usage guidelines or restrictions to access the model or implementing safety filters.
- Datasets that have been scraped from the Internet could pose safety risks. The authors should describe how they avoided releasing unsafe images.
- We recognize that providing effective safeguards is challenging, and many papers do not require this, but we encourage authors to take this into account and make a best faith effort.

12. Licenses for existing assets

Question: Are the creators or original owners of assets (e.g., code, data, models), used in the paper, properly credited and are the license and terms of use explicitly mentioned and properly respected?

Answer: [Yes]

Justification: We cite all assets used in the paper.

Guidelines:

- The answer NA means that the paper does not use existing assets.
- The authors should cite the original paper that produced the code package or dataset.
- The authors should state which version of the asset is used and, if possible, include a URL.
- The name of the license (e.g., CC-BY 4.0) should be included for each asset.
- For scraped data from a particular source (e.g., website), the copyright and terms of service of that source should be provided.
- If assets are released, the license, copyright information, and terms of use in the package should be provided. For popular datasets, paperswithcode.com/datasets has curated licenses for some datasets. Their licensing guide can help determine the license of a dataset.
- For existing datasets that are re-packaged, both the original license and the license of the derived asset (if it has changed) should be provided.

- If this information is not available online, the authors are encouraged to reach out to the asset's creators.

13. New assets

Question: Are new assets introduced in the paper well documented and is the documentation provided alongside the assets?

Answer: [NA]

Justification: This paper does not release new assets.

Guidelines:

- The answer NA means that the paper does not release new assets.
- Researchers should communicate the details of the dataset/code/model as part of their submissions via structured templates. This includes details about training, license, limitations, etc.
- The paper should discuss whether and how consent was obtained from people whose asset is used.
- At submission time, remember to anonymize your assets (if applicable). You can either create an anonymized URL or include an anonymized zip file.

14. Crowdsourcing and research with human subjects

Question: For crowdsourcing experiments and research with human subjects, does the paper include the full text of instructions given to participants and screenshots, if applicable, as well as details about compensation (if any)?

Answer: [NA]

Justification: No crowdsourcing experiments were conducted in this study.

Guidelines:

- The answer NA means that the paper does not involve crowdsourcing nor research with human subjects.
- Including this information in the supplemental material is fine, but if the main contribution of the paper involves human subjects, then as much detail as possible should be included in the main paper.
- According to the NeurIPS Code of Ethics, workers involved in data collection, curation, or other labor should be paid at least the minimum wage in the country of the data collector.

15. Institutional review board (IRB) approvals or equivalent for research with human subjects

Question: Does the paper describe potential risks incurred by study participants, whether such risks were disclosed to the subjects, and whether Institutional Review Board (IRB) approvals (or an equivalent approval/review based on the requirements of your country or institution) were obtained?

Answer: [NA]

Justification: No human subjects were involved in this study.

Guidelines:

- The answer NA means that the paper does not involve crowdsourcing nor research with human subjects.
- Depending on the country in which research is conducted, IRB approval (or equivalent) may be required for any human subjects research. If you obtained IRB approval, you should clearly state this in the paper.
- We recognize that the procedures for this may vary significantly between institutions and locations, and we expect authors to adhere to the NeurIPS Code of Ethics and the guidelines for their institution.
- For initial submissions, do not include any information that would break anonymity (if applicable), such as the institution conducting the review.

16. Declaration of LLM usage

Question: Does the paper describe the usage of LLMs if it is an important, original, or non-standard component of the core methods in this research? Note that if the LLM is used only for writing, editing, or formatting purposes and does not impact the core methodology, scientific rigorosity, or originality of the research, declaration is not required.

Answer: [NA]

Justification: The paper does not describe any usage of LLMs as a core method in this research.

Guidelines:

- The answer NA means that the core method development in this research does not involve LLMs as any important, original, or non-standard components.
- Please refer to our LLM policy (<https://neurips.cc/Conferences/2025/LLM>) for what should or should not be described.